CCSBT-ESC/2409/21
(ESC Agenda item 7.1 and 8)

Update of CPUE abundance index using GAM for southern bluefin tuna in CCSBT up to the 2023 data

CCSBT のミナミマグロについての GAM を用いた CPUE 資源豊度指数の 2023 年データまでの更新

Tomoyuki ITOH and Norio TAKAHASHI
伊藤智幸・高橋紀夫
Fisheries Resources Institute, Japan Fisheries Research Agency
水産研究･教育機構 水産資源研究所

要約

2022 年 ESC27 では、GAM を用いた 2 段階のデルタログノーマルアプローチで CPUE を標準化して、面積重みづけする新たなミナミマグロの CPUE 資源量指数の作成方法に合意した。合意された方法に従い、CPUE 資源量指数の作成を 2023 年までの漁獲データに対して実施した。本文書ではベースケースの結果と、様々な感度分析を行った結果を示す。得られた指数値では 2022 年に中程度に増加し、2023 年には少し低下した。モデル選択、レトロスペクティブ解析、船の ID、海域範囲の変更、対象年齢の変更、データおよびモデルの分解能の変更を含む様々な感度分析に対して資源量指数は頑健であった。操業の無い時空間に対する予測 CPUE が高い値を示す場合があった。

Summary

At ESC27 in 2022, the new calculation method of the abundance index of southern bluefin tuna, which standardized by generalized additive model in the two-step delta log normal approach with area weighting, was agreed. The CPUE abundance index was updated for fishery data up to 2023 according to the agreed methodology. This document presents the base case results as well as the results of various sensitivity tests. The index value was increased moderately in 2022 and decreased slightly in 2023. The abundance index was robust for a variety of sensitivity analyses, including model selection, retrospective analysis, vessel ID, area range changes, age range changes, and data and model resolution changes. There were cases where the predicted CPUE for non-fishing space-time showed high valuess.

1. Introduction

Stock assessment and stock management through the Management Procedure (MP) of southern bluefin tuna (*Thunnus maccoyii*; SBT) in CCSBT have historically been strongly relied on the abundance index obtained from the CPUE (number of fish / 1000 hooks) of the Japanese commercial longline fishery. In the old days, Nishida and Tsuji (1998) developed a model to calculate the abundance index by the generalized linear model (GLM). Since 2007, alternative abundance index was developed which called the core vessel CPUE standardized by GLM in response to the shrinking operating area in time and space and the problem of target fish species (ESC12 report, Itoh et al. 2008). The CPUE abundance index had been used as one of the main abundance indices in the two MPs of the Bali procedure used for the TAC calculation from 2012 to 2020 and the Cape Town Procedure (CTP) used for the TAC calculation from 2021.

It was recognized that the 2018 value of the CPUE abundance index by the core vessel CPUE was anomalously high in ESC24 held in 2019 (ESC24 Report). This prompted further investigation, which subsequently identified that this estimate was generated due to a prediction bias in the GLM standardisation method being used, which generated anomalously high estimates for cells with no effort. At ESC26 in 2021, it was agreed that a new CPUE abundance index should be prepared by May 2022 to assess its impact on MP (ESC26 report). Through the collaboration work between Japanese scientists and the consultant hired by CCSBT, as well as the discussion and suggestion of the CPUE working group, a new abundance index using CPUE standardised by the generalized additive model (GAM) was developed and agreed at ESC27 in 2022 (OMMP12 and ESC27 Reports).

This document presents the CPUE results obtained by updating the data to 2023 using the agreed GAM methodology not only for the base case but also for the various sensitivity analyses (Itoh and Takahashi 2022, 2023a). Although the ESC has already agreed to use the GAM new series in 2023, the CPUE abundance index may change with additional updates of the data over a one-year period, we need to carefully consider whether we can draw the same conclusion again. We have done all the analyses which had been done last year (Itoh and Takahashi 2023a). We have also included in this document a detailed review of predicted value from model conducted last year (Itoh and Takahashi 2023b).

2. Materials and Methods

2-1. Dataset used

The dataset was extracted from logbook data for the Japanese longline fishery, which include the period from 1969 to the latest year (currently 2023). Following procedures for the conventional SBT CPUE abundance index, records in statistical Areas between 4 and 9 and from April to September were selected. From the logbooks, year, month, latitude (in 1 degree), longitude (in 1 degree), vessel ID (available from 1979), number of hooks used, number of fish caught of SBT, bigeye tuna (*T. obesus*, BET), yellowfin tuna (*T. albacares*, YFT), albacore (*T. alalunga*, ALB) and swordfish (*Xiphias gladius*, SWO) data were used. In the development work in 2022, the number of hooks between floats (HBF; available since 1975) and other fish species (several species of marlines, and butterfly kingfish (*Gasterochisma melampus*; available since 1994)) were examined and we decided not to use them so that these items were not included in the work this year.

From the size data of the CCSBT database, the age composition of Japanese commercial catch was calculated and converted into the number of fish caught age-4 and older (age-4 plus). The age composition information was first applied to the fork length composition of 50 or more individuals measured in the same month, 5 degrees longitude, and 5 degrees latitude. At this stage, 97% of the number of SBT caught

was incorporated and the ratio of age-4 plus was calculated. For records of the conditions for 50 or more individuals were not met the time and space were gradually expanded to correspond to fork length composition, such as the same month - longitude 15 degrees - latitude 5 degrees, the same month - longitude 15 degrees - latitude 15 degrees, the same quarter - longitude 15 degrees - latitude 5 degrees, the same quarter - Statistical Area, and the same year - Statistical Area, and the same year. The fork length was converted to age by the age-length relationship used by CCSBT. Sensitivity analysis was conducted for age-5 plus and all ages.

The following records were eliminated: hooks 500 or less, hooks 4500 or more, CPUE 200 or higher. As a result of the examination, with the agreement in the CPUE working group discussion, the record of 50S (50S to 54S), which had a small number of data, were also eliminated.

2-2. Cluster analysis

A cluster analysis was performed to consider the target species of the fishing operations. The *clust_PCA_run* function of the R package *cpue.rfmo* was used. Cluster analysis was performed using the number of fish caught of five species, SBT, BET, YFT, ALB and SWO as data.

2-3. Standardization by GAM

Standardization by the generalized additive model (GAM) was carried out by use of the delta log normal approach. A software for statistical computing and graphics, R was used for analysis. The *bum* function, which is suitable for large volumes of data, in the *mgcv* package was used. Based on the results of the study by the consultant (Dr. Hoyle), a binomial submodel (hereinafter referred to as BSM) and a positive catch submodel (hereinafter referred to as PCSM) were used, and gamma = 2, binomial distribution and gauss distribution were used respectively (Hoyle 2022). For the smoother, s (spline) was used for the offset term (hook logarithmic value), and ti (tensor product suitable when there was an interaction with the main effect) was used for the others. cs (cubic regression spline with shrinkage) was used for the basis function (bs) of ti. Gamma is a coefficient multiplied by EDF (described later) and promotes smoothing with values set to >1 (= 1.5 is common).

Binomial submodel

```
cpue > 0 ~ yf +ti(month) + ti(lon) + ti(lat) +
    ti(lon,  lat) + ti(month, lat) + ti(lon, month) + ti(year, lat) + ti(year, lon) + ti(year, month) +
    cl + s(log(hook))
```

Positive catch submodel

```
log(cpue) ~ yf +ti(month) + ti(lon) + ti(lat) +
    ti(lon,  lat) + ti(month, lat) + ti(lon, month) + ti(year, lat) + ti(year, lon) + ti(year, month) +
    ti(lat, month, year) + ti(lat,  lon, month) + ti(lat, lon, year) + ti(year, lon, month) +
    cl + s(log(hook))
```

where,

yf: Year of fishing. In factor.

year: Year. In number

month: Month. In number

lat: Latitude in 5 degree. In number. Represented by the middle (e.g. -47.5 from 45.0S to 49.9S)

lon: Longitude in 5 degrees. In number. Represented by the middle (e.g. 32.5 for 30.0E to 34.9E). Convert to 360 degree while >240 was converted by -360 so that lon ranged from -22.5 to 187.5 continuously.

cl: Cluster. In factor. 1, 2, 3, and 4.

hook: Number of hooks used. In number.

R code actually used is as follows.

Binomial submodel

```
modA2 <- cpue > 0 ~ yf +
                        ti(month,        k=kA.month11,bs="cs")+
                        ti(lon,          k=kA.lon11,bs="cs")+
                        ti(lat,          k=kA.lat11,bs="cs")+
                        ti(lon,  lat,    k=c(kA.lon21,  kA.lat21), bs="cs")+
                        ti(month, lat,   k=c(kA.month22,kA.lat22), bs="cs")+
                        ti(lon, month,   k=c(kA.lon23,  kA.month23), bs="cs")+
                        ti(year, lat,    k=c(kA.year24, kA.lat24), bs="cs")+
                        ti(year, lon,    k=c(kA.year25, kA.lon25), bs="cs")+
                        ti(year, month,  k=c(kA.year26, kA.month26), bs="cs")+
                        cl+
                        s(log(hook))
mgcv::bam(modA2, data =data, gamma = 2, method = 'fREML', family = binomial, discrete=F)
```

Positive catch submodel

```
modB3 <- log(cpue) ~ yf +
                        ti(month,            k=kB.month11,bs="cs")+
                        ti(lon,              k=kB.lon11,bs="cs")+
                        ti(lat,              k=kB.lat11,bs="cs")+
                        ti(lon,  lat,        k=c(kB.lon21,  kB.lat21), bs="cs")+
                        ti(month,lat,        k=c(kB.month22,kB.lat22), bs="cs")+
                        ti(lon,  month,      k=c(kB.lon23,  kB.month23), bs="cs")+
                        ti(year, lat,        k=c(kB.year24, kB.lat24), bs="cs")+
                        ti(year, lon,        k=c(kB.year25, kB.lon25), bs="cs")+
                        ti(year, month,      k=c(kB.year26, kB.month26), bs="cs")+
                        ti(lat,  month,year, k=c(kB.lat31, kB.month31, kB.year31), bs="cs")+
                        ti(lat,  lon, month, k=c(kB.lat32, kB.lon32, kB.month32), bs="cs")+
                        ti(lat,  lon, year,  k=c(kB.lat33, kB.lon33, kB.year33), bs="cs")+
                        ti(year, lon, month, k=c(kB.year34, kB.lon34, kB.month34), bs="cs")+
                        cl+
```

s(log(hook))

mgcv::bam(modB3, data = data.positive, gamma = 2, method ="fREML", discrete=F)

The larger the k value (basis dimension for smoothing flexibility) of the interaction, the better, but the longer the calculation time (Wood, help of *choose.k* in mgcv). The effective degrees of freedom for a model term (EDF) value is calculated by the *k.check* function in mgcv package, and if EDF was close to k' (the maximum possible EDF for the term), "and" the p-value of k-index is < 0.05, a larger k value was set. The k values were determined by trial and error. Since the k value of the interaction is treated as the value of 2 multiplications (3 multiplications for 3 interactions), it is not necessary to set them separately, however, for the purpose of organizing the work, the k value of each variable in the interaction was set to the same value (i.e. k for year = 20 was used for all interaction terms which include year).

For the diagnosis of the GAM result, the fit was confirmed by the plot diagram (QQ plot, residual distribution) by the *gam.check* function of the mgcv package. AIC was calculated. The distribution of the residuals for each variable was examined. It was examined whether the predicted values were consistent with our knowledge of distribution of SBT and plausible trend of SBT stock abundance. We made a comprehensive judgment by looking at these information as well as AIC.

Calculation is performed by desktop PC (CPU = Intel (R) Core (TM) i9-10900T CPU @ 1.90GHz and 1.90 GHz, RAM = 64.0GB, 64 bit, Windows 10 Pro). The software R (R4.1.2) was used to make the dataset. Microsoft R Open 4.0.2 was used to calculate GAM.

2-4. Calculation of abundance index

After creating data with all combinations of year / month / latitude / longitude (using R's *expand.grid* function), we made a dummy data set limited to the month / latitude / longitude where the fishing was operated in the past. The predicted value was calculated for each submodel for the dummy data set, and the product of estimates from the two submodels (BSM and PCSM) was calculated. Since the expected value is biased when the lognormal distribution is restored, the predicted value was corrected by adding mean squared error (MSE) / 2 in the case of the positive catch submodel.

Furthermore, the area weighting coefficient was calculated in consideration of the fact that the distance of 1 degree of longitude differs depending on the latitude and the number of 1 degree squares that SBT have been caught in the past within the 5 degree x 5 degree squares. The abundance index can be calculated by the following formula.

Σ(predicted value of binomial submodel of dummy data set × predicted value of positive catch submodel of dummy data set × Area weighting coefficient) / Overall average value.

2-5. Sensitivity analysis

Various sensitivity analyses were performed along the way in selecting the datasets and methods. The following sensitivity analyses were performed at the final stage in 2022 and updated in 2023. We repeated the same procedure for the 2024 work.

Model selection: In some cases, estimation did not converge, and in some cases, even if the AIC was low, the abundance index behaved significantly differently from the others, so a simple selection by AIC seemed inappropriate. For the binomial submodel, we tried the case where all the interactions were removed from the base case, the case where the two-way interaction was removed one by one, and the case where the three-way interaction was added one by one. For the positive catch submodel, we tried the case where all the interactions were removed from the base case, the case where the two-way interaction was

removed one by one, and the case where the three-way interaction was removed one by one.

Retrospective analysis: Excludes data from the last year up to the past 10 years. It was also carried out in a part of the sensitivity analysis (i.e. latitude-longitude resolution in the model, core vessel). Mohn's rho was calculated as an index of retrospective bias (Hurtado-Ferro et al. 2015).

Selection of k: Effect when k was increased by one step.

Effect including vessel ID: The effect of including vessel ID in each of BSM and PCSM.

Effect excluding 30S: We saw the effect excluding 30S from the dataset.

Effect of changing age: Age-4 plus used in the base case, but limited to age-5 plus, or all ages were tried.

Data resolution: The shot-by-shot data are used in the base case. Aggregated data by month, 1 degree latitude and 1 degree longitude, and aggregated data by month, 5 degrees latitude and 5 degrees longitude were tried.

Latitude-longitude resolution in the model: The latitude and longitude in the model is based on the 5-degree in the base case. We tried the effect when this was made into one degree resolution.

2 clusters: 4 clusters were the base case, but we tried clusters in 2 groups.

Core vessel: From the dataset prepared for this analysis (note that it differs from the traditional GLM dataset), we tried to select core vessels and create CPUE index. A core vessel is defined as a vessel that has been included in the top *xx* rank in terms of SBT catch in number of *yy* years.

2-6. Abundance indices by historical models

We compared the newly created abundance index (GAM_new) with other models used in CCSBT including the core vessel index by the conventional GLM (GLM_core) and the one obtained by GAM used for the 2020 stock assessment (GAM11).

The GLM model is as follows (Itoh and Takahashi 2022):

$$log(CPUE+0.2) = Intercept + Year + Month + Area + Lat5 + BET\_CPUE + YFT\_CPUE + (Month*Area) + (Year*Lat5) + (Year*Area) + Error,$$

where year, month, area, lat5 were treated as factors. A Gaussian distribution was used for the error term. *glm* function of R was used. Note that whole the dataset was applied instead of restricted to the core vessel data.

The GAM11 models is as follows:

$$log(CPUE +0.2) = Intercept + Year + te(Lon, Lat) +te(Lon, Month) = te(Year, Lat) + te(Year, Month) + te(Lat, Lon, Month) + te(Lat, Lon, Year) + s(BET=CPUE) + s(YFT\_CPUE) + Error.$$

A Gaussian distribution was used for the error term. W0.8, which weighed indices of 80% constant and 20 % variable square hypotheses, was used for these indices.

2-7. Analysis of predicted value

To each record of the dummy data set, the number of operations in actual fishery data was attached. Predicted values were calculated for each combination of variables by GLM (GLM_core) and GAM (GAM_new), respectively (both area weighted). The dataset was classified into four groups based on the number of operations actually given. Group 0 has 0 operations, Group 1 has 1 to less than 5 operations, Group 2 has 5 to less than 10 operations, and Group 3 has 10 or more operations.

A higher CPUE is expected in a space-time with a higher number of operations. This is because there would be a high probability that a vessel does not stay in a space-time with a low CPUE, and it is expected that operations are not conducted in a space-time with a low CPUE through the accumulation of historical knowledge. Boxplot is used for visualization.

3. Results

3-1. Dataset used

Data from 1969 to 2023 amounted to 803,439 records. Of these, 710,182 records included catch of SBT age-4 plus, accounting for 88% of the total. A fairly high positive catch rate is characteristic of this dataset. By year, the positive catch rate dropped to about 60% in the mid-1990s and around 2010, but otherwise remained above 80% (Fig. 1). The percentage was high in 2023, and few low values were observed in the aggregated month and 5-degree data (Fig. 1, center panel). The nominal CPUE of the positive catch dataset is high in the 1970s, low in the 1980s to 2000s, and high after 2010. The nominal CPUE in 2022 was the highest in the past 40 years and slightly decreased in 2023.

Similar figures are shown for other variables, including month, longitude, latitude, latitude and longitude maps (Fig. 2 and Fig. 3). There is no strong tendency for the month and longitude. For latitude, positive rate and CPUE in the positive catch data was low at 30S, high up to 35S (CPUE) or 40S (positive rate), and 45S was similar to 40S. Data of 30S exists only in the Pacific Ocean (Area 4 and Area 5).

3-2. Cluster analysis

The data were divided into four cluster groups. Relevant figures are shown in Fig. 4 to Fig. 8. Since the eigenvalues are greatly reduced to 2 groups and the decrease to 4 groups is not so large, it may be appropriate to divide them into 2 groups. However, in the analysis of the data up to 2020, there was a problem that the BSM of GAM did not converge when divided into two groups (the data up to 2021 converged in a short time). Therefore, we decided to analyze in 4 groups. Note that the case of 2 groups was carried out by sensitivity analysis.

The fish species included five species: SBT, BET, YFT, ALB and SWO. At the stage of trial and error in the 2022 work, we also tried 3 species (SBT, BET and YFT) and obtained the similar results as 5 species. But 3 species are few and cover all species that can be the main target of operation, it was decided by the CPUE working group to have 5 species (Itoh and Takahashi 2022).

The latitudes of the four clusters differed (Fig. 7), however, there were no noticeable trends in year, month, longitude, number of hooks used, or hooks between floats (HBF). It was probable that HBF had a narrow range in the dataset and did not make a difference because it contained few data of deep longline targeting on BET. Such an effect may have been seen in the waters north of the Area 4-9. The main catch in the first cluster which locate southernmost was SBT. SBT and ALB were caught in the second cluster. The third cluster was a mixture of SBT, ALB and BET and the fourth cluster was a mixture of five species.

3-3. Standardization by GAM

For the binomial submodel, the model including all main effects and two-way interaction terms was selected mainly from AIC in the 2022 work. There was a problem that the run did not converge when the three-way interaction term was included. For the positive catch submodel, the model including the main effect and all the two-way and three- way interaction terms was selected mainly from AIC. It was agreed in the ESC in 2022 that these models were used for the base case.

The k value was examined independently for each submodel. The same sets of k used in the 2022 work

were utilized (Table 1). Table 2 shows relevant statistics including the EDF value for k and the p value for k-index. There are cases where EDF is close to k' (e.g. positive catch submodel ti (lat)), but since the p value is well above 5% in that case, k is large enough and there is no problem.

The diagnosis results are shown in Table 3, Fig. 9, and Fig. 10. The binomial submodel explained 73.7% deviance, and the positive catch submodel explained 49.5%. For BSM, the QQ plot is generally good, although some parts do not fit at both ends. The residual histogram has a single peak and is skewed to near 0 residual. For PCSM, the QQ plot is generally good, and the residual has a single peak. In the plot of the fit value and the response variable, there is a roughly upward-sloping relationship. Both are judged to be not bad fit.

The residuals were further examined. Plots were made for year, month, latitude, and longitude (Figs. 11 and 12). Note that these figures are not from *gamVis*, which uses simulation. There was too much data and *gamVis* caused a memory over and so we couldn't get any results. These are simple box plots of residuals. For BSM, the median residuals were positively biased in 2004-2007 in the year. There was a slight positive bias for month. At latitude, the negative bias was large at 30S, a slight positive bias was seen at 35S, and the bias was small at 40S and 45S. At the western end of the longitude, there was a large negative bias.

For PCSM, the bias was small by year and month. At latitude, the range was large at 30S. The bias of the longitude was small, but a negative bias was seen only at the eastern end. When made into a map, the area with zero residuals was greatly expanded in both submodels (Fig. 13). In some places, large residuals may occur in the peripheral waters. It has been confirmed in the 2022 work that the data in the area where these large residuals are seen has almost no effect on the abundance index.

Box plots of predicted values for variables (year, month, latitude, longitude, latitude x longitude) are shown (Fig. 14, Fig. 15, Fig. 16, Fig. 17 and Fig. 18). No inconsistency was found in comparison with the current knowledge of the distribution of SBT and changes in the abundance. The predicted values by year in the BSM (top panel of Fig. 14) ranged from 0% to 100%, which is quite different in appearance from the 2023 work, where only 90% or more appeared. This is because the GAM parameter estimates are relative values based on the most recent year, and the nominal value for the 2023 data is concentrated at 100%. The high median of the predicted values for each year, at 90%, is common to the output of the 2023 work. The high predicted values in the southeastern waters of Australia (35S, 140E) are interesting (Fig. 18). Currently, there is no fishing operation in this area, but it was confirmed in the 2022 work that the fishing was operated in this area in the 1970s and 1980s.

3-4. Calculation of abundance index

The predicted value of the dummy data set was weighted by the area factor and normalized by the average value to obtain the abundance index. To see the effect of area weighting, we compared it with a simple unweighted average (Fig. 19). As a result, it was found that they are similar to each other and the influence of weighting is small. Since this method includes the interaction of years in the model, it is no longer necessary to obtain the conventional Constant / Variable square hypothesis and its intermediate index (see Hoyle (2022) for details).

Figure 20 shows the obtained abundance index. The values are shown in Table 4. It increased in many years from 2006 to 2022. In 2023, it decreased from 2022 but higher than 2021 in the series.

3-5. Sensitivity analysis

Model selection

For BSM, a model (modA2) containing all two-way interactions was selected as the base case in the 2022 work. Its AIC was lower than any other model with one term removed from modA2 (Table 5). On

the contrary, in the model to which one three-way interaction term was added (e.g. modA2.p11), the AIC was low, but there was a problem that it did not converge sometimes. The difference on the abundance index was small in the models (Fig. 21 and Fig. 22). Therefore, it is considered appropriate to use modA2 as the base case this year again.

For PCSM, a model (modB3) containing all the two-way and three-way interaction terms was selected as the base case in the 2022 work. Its AIC was lower than any other model with one term removed from modB3 except modB3.no8 (Table 6). In order to maintain consistency, modB3 was used as the base case this year again. The difference between the models in the abundance index is small (Fig. 23 and Fig. 24). Relatively large differences were seen in modB3.no9 and mdB3.no10 which excluding ti(year, lon) and ti(year, month), respectively.

Retrospective analysis

Figure 25 shows the results of retrospective analysis of the base case model. Figure 26 shows the results by each submodel. The value for 2022 was a large overestimate. Differences were smaller for previous years. Mohn's rho was 0.16, less than the +0.20 that indicates caution (Hurtado-Ferro et al. 2015).

We examined further for the 2022 value. We compared the results of the data up to 2022 made in 2023 and that in 2024. That is, verification of the additional effect of data for 2022. As a result, the value for 2022 was even higher in the 2024 dataset (Fig. 27). These indicate that the evaluation of the most recent year of data is sensitive to the addition of the data for the following year.

Selection of k

For BSM, we examined the effect of adding +1 to k of the month, +5 to k of the year, and +5 to k of the longitude. The latitude has already reached the maximum value (k = 4). For PCSM, we examined the effect of increasing the year k by +5 and the longitude k by +5. The month and latitude are already at their maximum.

As a result, there was very little effect on BSM (Fig. 28 and Fig. 29), however, there is some change when kA.year25 (ti(year, lon)) was changed from 10 to 15. It is suggested that k was large enough for most cases. For PCSM, there was a noticeable change when kB.year34 (ti (year, lon, month)) or kB.year33 (ti (lat, lon, year)) was changed from 20 to 25 (Fig. 30, Fig. 31). It might be better to consider increasing these k-values associated with year in future.

Effect of including vessel ID

The vessel ID was included in the logbook data after 1979. The analysis was limited to the data in the years after that and records that the vessel ID was not missing. We tried both cases where the vessel ID was included as a fixed effect and where it was included as a random effect. Both cases took a long time to calculate. Whereas the base case took 30 minutes, the random term took more than 120 minutes, and the fixed effect took more than 155 minutes.

The results are shown in Fig. 32. The trajectories of the three abundance indices were similar to each other, which suggests the effect including the vessel ID was small. However, the behavior of recent years differs depending on the model and index with vessel ID had larger values in 2022 and 2023. Due to the long run time, it was not possible to conduct a more detailed examination by trial and error.

Effect of excluding 30S

In the dataset used, 30S existed only in the Pacific Ocean in Statistical Area 4 and 5. As a test, data in 30S was eliminated from the dataset for the base case. The cluster analysis has not been redone. The abundance index is shown in Fig. 33. The abundance index is similar to each other. While there was a large difference in the 2022 value in the 2023 work, there is little difference in the 2024 work.

Effect of changing age range

The results are shown for the base case of age-4 plus, limited to age-5 plus (Fig. 34), and for all ages (Fig. 35). At the age-5 plus, the overall trajectory was similar to the base case up to 2021, but significantly lower in 2022 and 2023 values. For all ages, the values for 1990-1994 and 2017-2023 were higher, but the overall trajectory was similar.

This sensitivity analysis is related to release and discard. When fish is released and discarded from longline vessels, it is often a small fish, age-3 or age-4. The proportion of released fish will depend not only on the vessel's IQ utilization strategy but also on the cohort strength. If the proportion of released fish changes in a certain year in the future, the effect can be examined by calculating the abundance index for those ages other than 4 and comparing it with the abundance index for those age-4 plus.

Resolution of data

The base case was obtained from shot-by-shot data. On the other hand, Fig. 36 shows the comparison with the aggregated data by month in 5 degrees x 5 degrees, and Fig. 37 shows the comparison with the aggregated data by month in 1 degree x 1 degree. The abundance index in the 5-degree aggregated data behaved differently from that in the shot-by-shot data after 2014. This is probably due to differences in the amount of data and effort. In this analysis, CPUE is taken as a response variable, and the number of hooks used is included as an offset term by taking a logarithm. For this reason, in the 5-degree aggregate data, even if there are multiple operations, they are treated as one record, and the effect of the number of operations (number of hooks) is treated only in logarithmic. Shot-by-shot data influences the results according to the number of operations. That is, aggregated data underestimates the variance in CPUE fluctuations. The abundance index of 1-degree aggregated data was an intermediate characteristic between shot-by-shot and 5-degree aggregated data.

The residuals were plotted against four variables (year, month, latitude, longitude) (Fig. 38). A significant improvement was seen in the homoscedasticity of the residuals by using shot-by-shot at latitude. From these facts, the resolution of the data has a strong influence on the result, and it is considered appropriate to use shot-by-shot data as agreed in 2022.

Resolution in the model in latitude and longitude

The latitude and longitude in the model uses a 5-degree resolution, but we tried the effect of using this as a 1-degree resolution. The runtime then doubled. The abundance index was higher in the 1-degree model in 2010-2015 and 2022-2023 (Fig. 39). When retrospective analysis was performed, the 1-degree model was more deviated and overestimation (Mohn's rho=0.22) than the base case (Fig. 40). By submodel, BMS was underestimated ant PCSM was overestimated (Fig. 41).

2 clusters

The base case used clusters in four groups, but clusters in two groups were tried. SBT was abundant in the first cluster, and five species were mixed in the second cluster. The first cluster was located to the south (Fig. 42, Fig. 43, Fig. 44, Fig. 45). The abundance index of two clusters was similar to that of four

clusters, although higher between 2018 and 2022 (Fig. 46). The 2022 work showed that the four clusters were considered more robust and suitable, as the dataset up to 2020 caused the problem of GAM convergence and there was no significant change in the abundance index.

Core vessel

The core vessel is that included in the top *xx* vessels in terms of SBT catch in number of a certain year and has been included for *yy* years. The conventional core vessel CPUE is selected with xx = 56 and yy = 3. The core vessel data set was obtained by setting xx and yy in various ways (Table 7). Data is limited to 1979 and later with vessel ID. The number of vessels selected has decreased from 3% to 17%. The abundance index is shown in Fig. 47. The behavior that deviated greatly was shown in the case of data in which the number of vessels was greatly compressed to <7%. The index values for 2022 and 2023 were lower on the core vessel.

Retrospective analysis was performed for the cases of core vessel data xx = 56 and yy = 3 (Fig. 48, Fig. 49). The result was roughly robust the data used, but was underestimated in 2013 and overestimated in 2020. Since the data was limited after 1979 because the vessel ID was required, and the robustness was inferior, it was considered that the significance of using the core vessel was small.

3-6. Comparison of abundance indices by historical models

We compared the newly created abundance index (GAM_new) with the core vessel index by the conventional GLM (GLM_core) and the one obtained by GAM used for the 2020 stock assessment (GAM11) (Fig. 50). The overall trends were similar to each other. Compared to the other two series, the new GAM series had lower values from 1970 to 1990. Also, the values were high in 1993-1994, 2019 and 2022. Values in 2022 was high and decreased in 2023 in GAM_new, while low in 2022 and high in GLM_core and GAM11. The value of 2023 was significantly high in GLM_core.

3-7. Analysis of predicted value

Figure 51 shows the proportion of each group of the number of operations conducted in the dummy dataset by year. The value for 2023 is provisional and may increase as data input work progresses. The proportion has decreased since 1969, indicating a decrease in the proportion of time-space in which operations took place. The decline has continued since 2000.

Figure 52 shows the predicted CPUE values by group in data all years combined, by GLM_core and GAM_new. As expected, the time and space with higher operation numbers had higher CPUE. The same figure is shown in Fig. 53, including the boxplot outlier. It is apparent that there are anomalously high predicted outliers in GLM_core and fewer in GAM_new.

A similar figure is shown in Fig. 54 by year. From 1969 to 2007, the box part is wide and the CPUE increases according to the increase in the number of operations. From around 2008, outliers became higher as the box area was compressed in the figure. From 2018, the outliers were particularly high in GLM_core, and it was significantly different from the figure by GAM_new. Fig. 55 shows the change in outliers over time in the space-time without operations. Extremely large outliers are seen in 2018 and 2019 in GLM_core and lesser extent in 2022 and 2023 in GAM_new. These came from Area 8 between June to September for GLM_core (Table 8) and Area 4 btween July and September for GAM_new (Table 9). Outliers in GAM are not extremely high.

4. Discussion

The 2023 fishing data was added to the dataset. The method using GAM agreed at the 2022 ESC was able to obtain a convergent solution without changing the settings such as the k parameter. For various sensitivity analyses, we were able to obtain results similar to those in the 2022 and 2023 works. The distribution of the residuals for each variable and the overall fitting of the residuals were the same as in the previous work, and no problems were observed. The results of the sensitivity analysis were similar to those of the 2022 and 2023 works.

The 2023 work resulted in fairly high values of 2022, while the 2024 work resulted in a more moderate increase in 2022 and a lower value in 2023. Caution is acknowledged that behavior of the most recent year may change with additional data in the following year. High CPUE was predicted in 2022 and 2023 for July to September in Area 4 where fishing was not conducted. Fishing in Area 4 is mostly conducted from April to June or July, and future data is unlikely to be available in the future. While this is not as significant an issue as the 2018 GLM_core, the predictions for the non-fished space-time will require careful interpretation and future monitoring.

5. References

CCSBT (2007) Report of the Twelfth Meeting of the Scientific Committee. 10 - 14 September 2007. Hobart, Australia. 80pp.

CCSBT (2019) Report of the Twenty Fourth Meeting of the Scientific Committee. 7 September 2019. Cape Town, South Africa. 121pp.

CCSBT (2021) Report of the Twenty Sixth Meeting of the Scientific Committee. 31 August 2021. Online. 93pp.

CCSBT (2022a) Report of the Twelfth Operating Model and Management Procedure Technical Meeting. 20-24 June 2022. Hobart, Australia and Online. 33pp.

CCSBT (2022b) Report of the Twenty Seventh Meeting of the Scientific Committee. 29 August-5 September 2022. Online. 114pp.

Hoyle, S. (2022) Validating CPUE model improvements for the primary index of southern bluefin tuna abundance. CCSBT-OMMP/2206/04.

Hurtado-Ferro, F., Szuwalski, C.S., Valero, J.L., Anderson, S.C., Cunningham, C.J., Johnson, K.F., Licandeo, R., McGilliard, C.R., Monnahan, C.C., Muradian, M.L., Ono, K., Vert-Pre, K.A., Whitten, A.R., Punt, A.E., (2015) Looking in the rear-view mirror: bias and retrospective patterns in integrated, age-structured stock assessment models. ICES J. Mar. Sci. 99–110.

Itoh, T., E. Lawrence, and J. G. Pope (2008) The development of new agreed CPUE series for use in future MP work. CCSBT-ESC/0809/09.

Itoh, T. and N. Takahashi (2022) Development of the new CPUE abundance index using GAM for southern bluefin tuna in CCSBT. CCSBT-OMMP/2206/08.

Itoh, T. and N. Takahashi (2023a) Update of CPUE abundance index using GAM for southern bluefin tuna in CCSBT up to the 2022 data. CCSBT-OMMP/2306/05

Itoh, T. and N. Takahashi (2023b) Further examination of CPUE abundance index using GAM for southern bluefin tuna based on predicted values. CCSBT-OMMP/2306/09.

Nishida T. and S. Tsuji (1998) Estimation of abundance indices of southern bluefin tuna (*Thunnus maccoyii*) based on the coarse scale Japanese longline fisheries data (1969-97).

CCSBT/SC/9807/13.

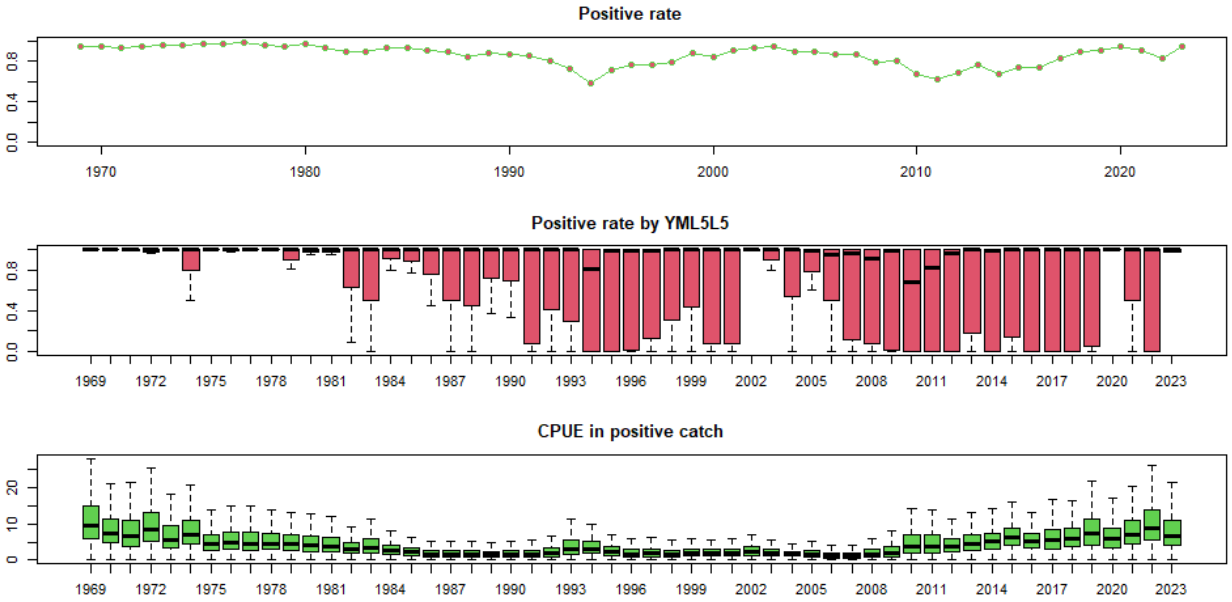

Fig. 1. Nominal value of positive catch rate and CPUE by year.
Upper panel is the positive rate which is the total number of positive catch operations / the total number of all records. Middle panels is boxplot based on the positive catch rate by year, month, 5 degree latitude and 5 degree longitude. Lower panel is CPUE in positive catch records.

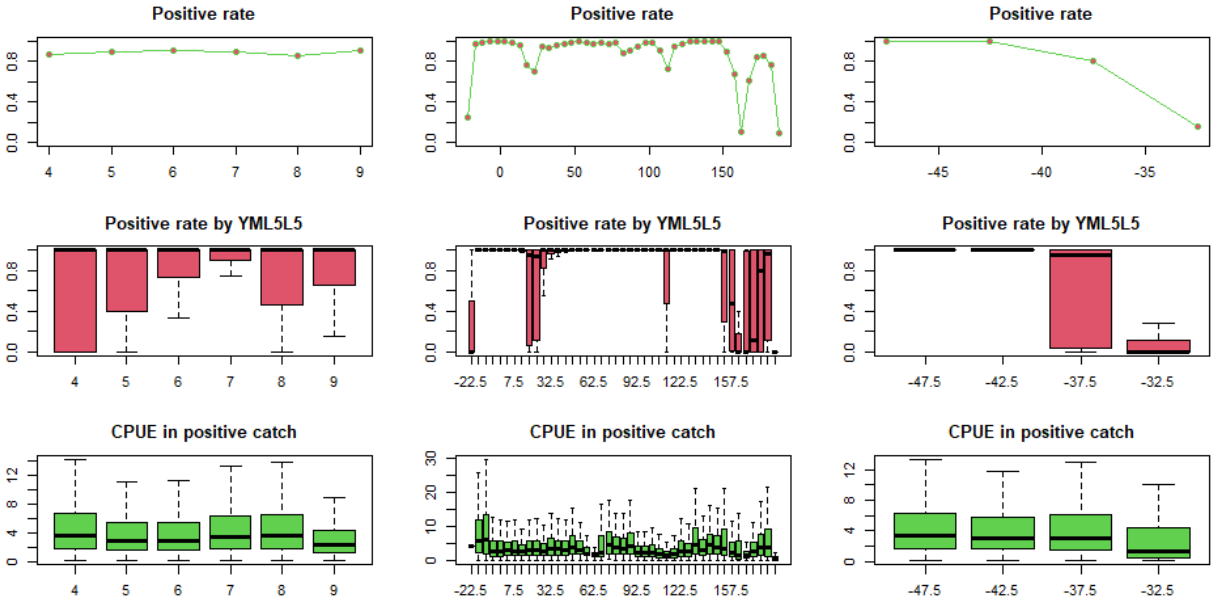

Fig. 2. Nominal value of positive catch rate and CPUE by month, longitude and latitude.
Upper panel is the positive rate which is the total number of positive catch operations / the total number of all records. Middle panels is boxplot based on the positive catch rate by year, month, 5 degree latitude and 5 degree longitude. Lower panel is CPUE in positive catch records.

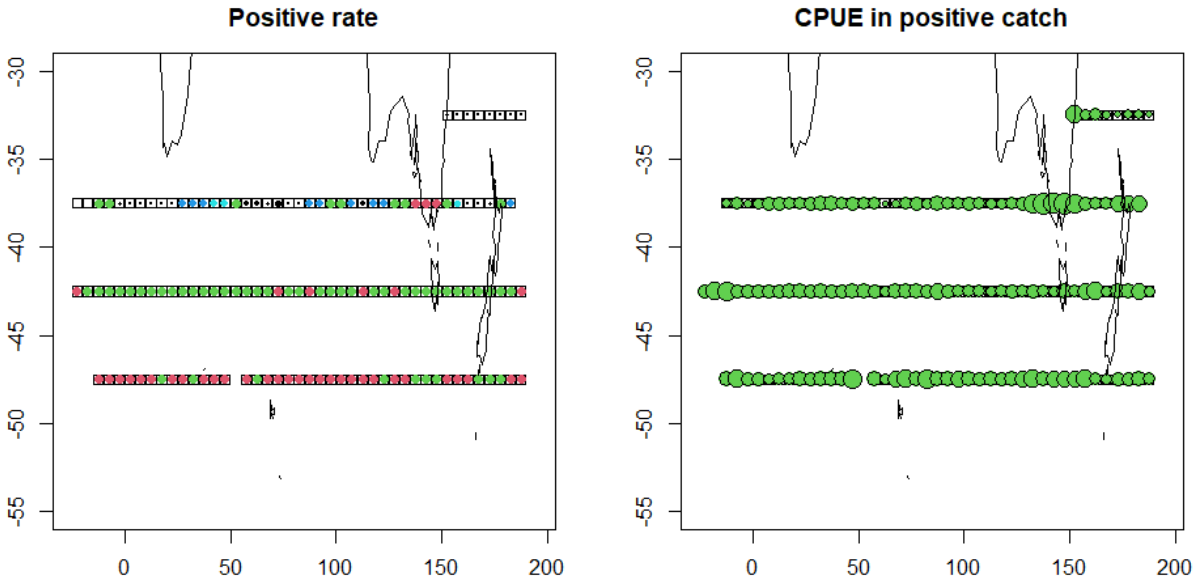

Fig. 3. Nominal value of positive catch rate and CPUE in map.
Left panel is the positive rate. Right panel is CPUE in positive catch records. Red is the higher value, followed by green, blue and white in the positive catch rate panel.

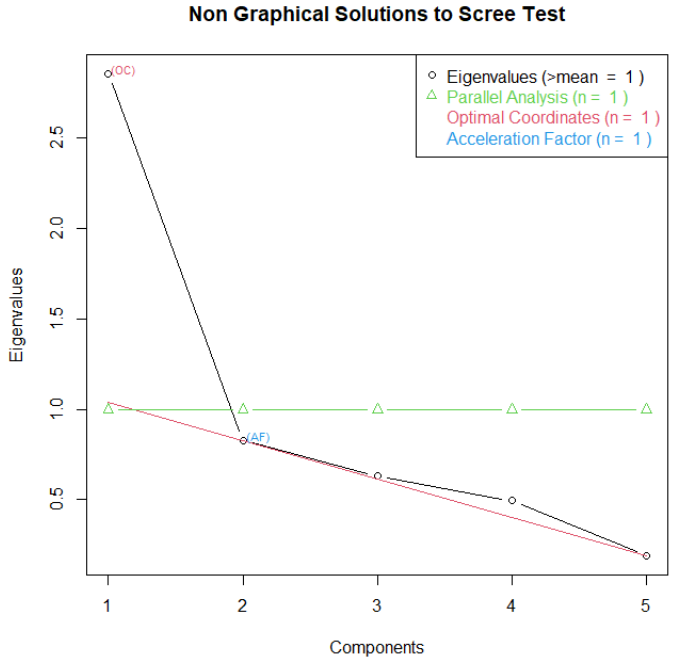

Fig. 4. Eigen values for the number of components in cluster analysis.

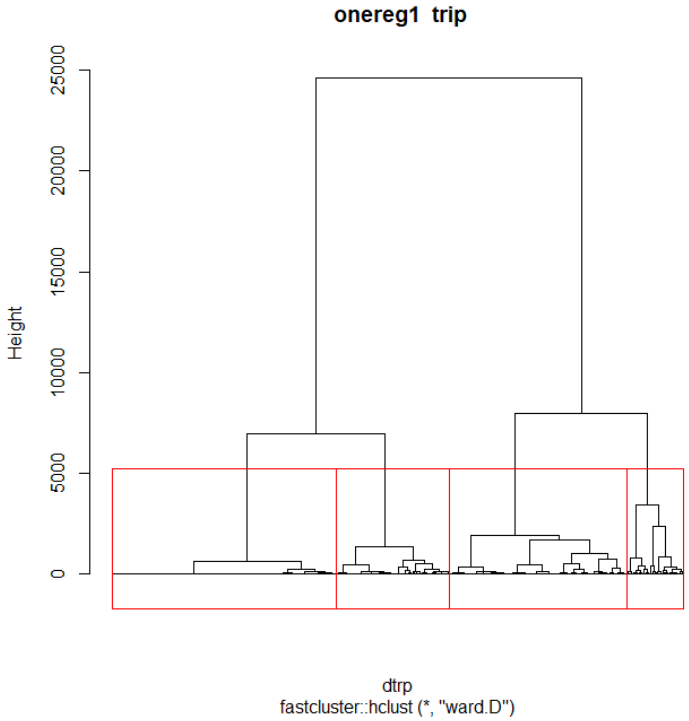

Fig. 5. Dendrogram of the cluster analysis.

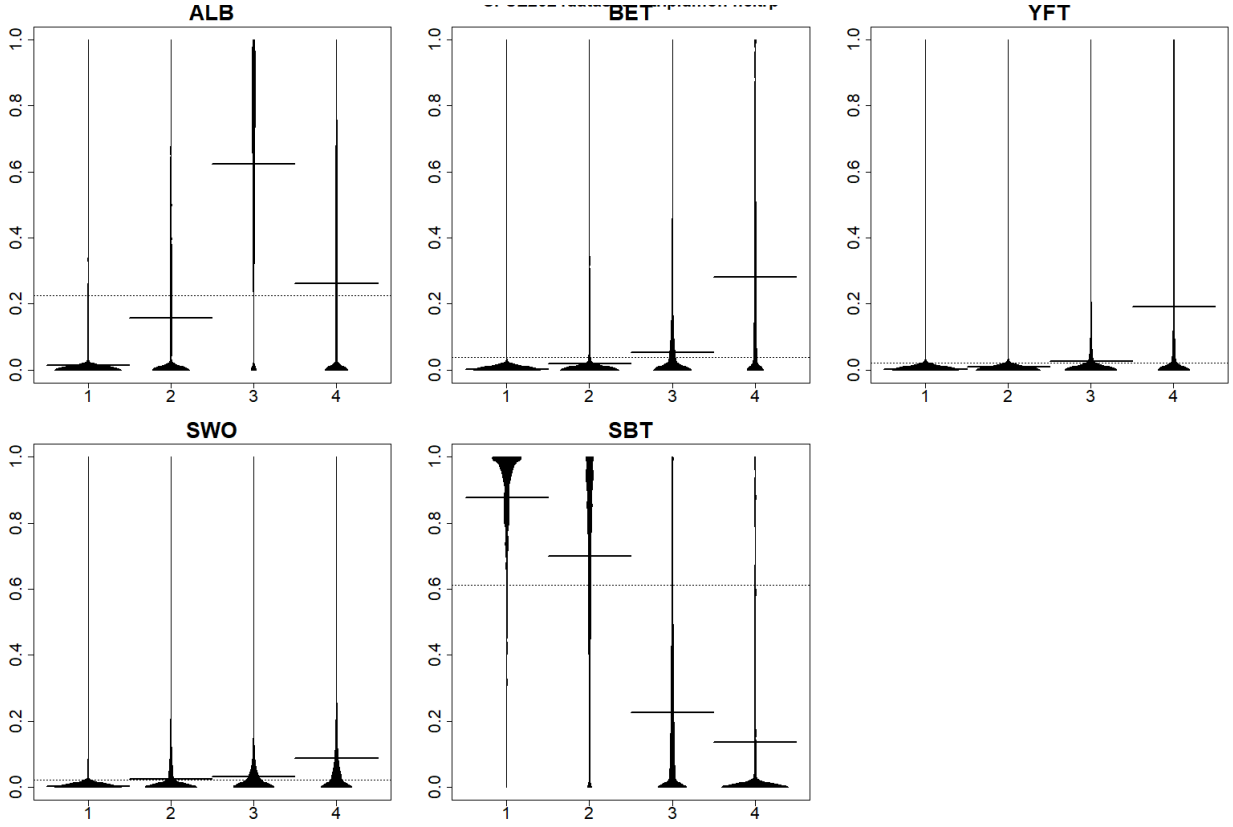

Fig. 6. Occurrence by species in each group in cluster analysis.
ALB is albacore, BET is bigeye tuna, YFT is yellowfin tuna, SWO is swordfish and SBT is southern bluefin tuna.

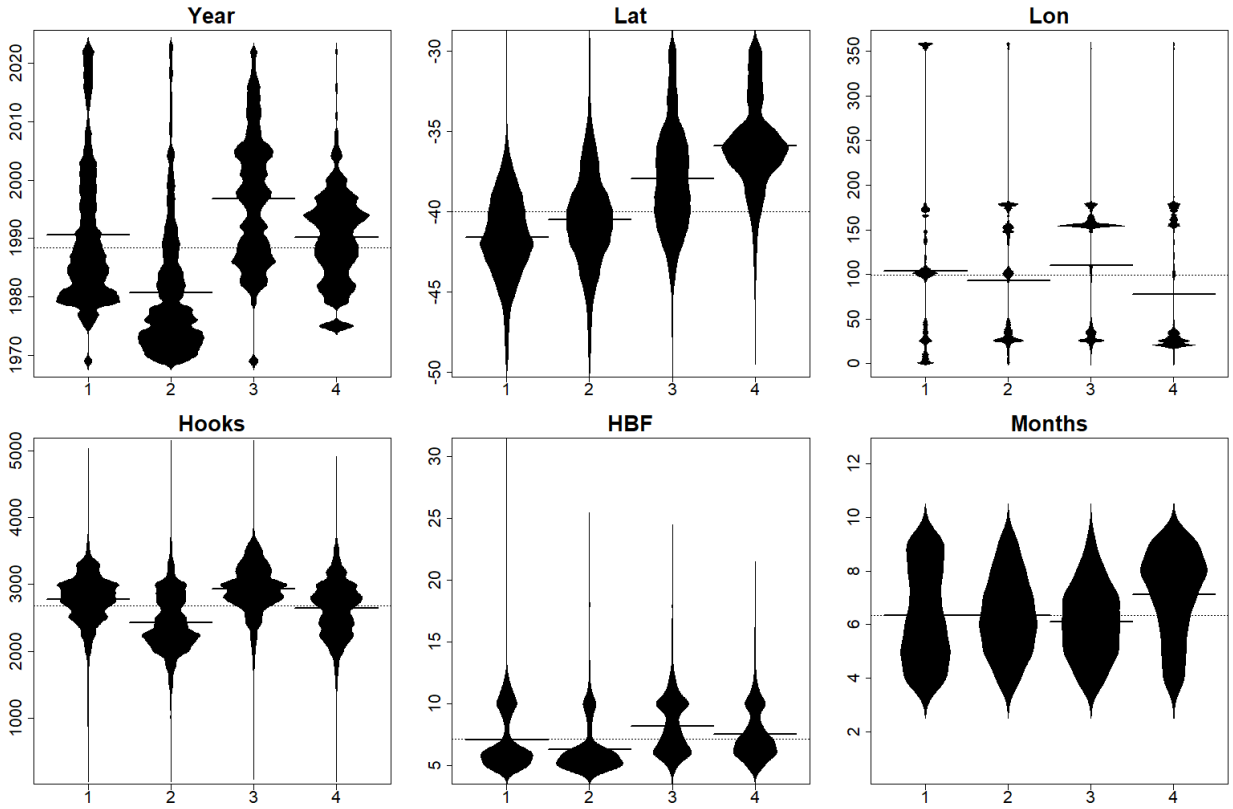

Fig. 7. Occurrence by variables of each group in the cluster analysis.

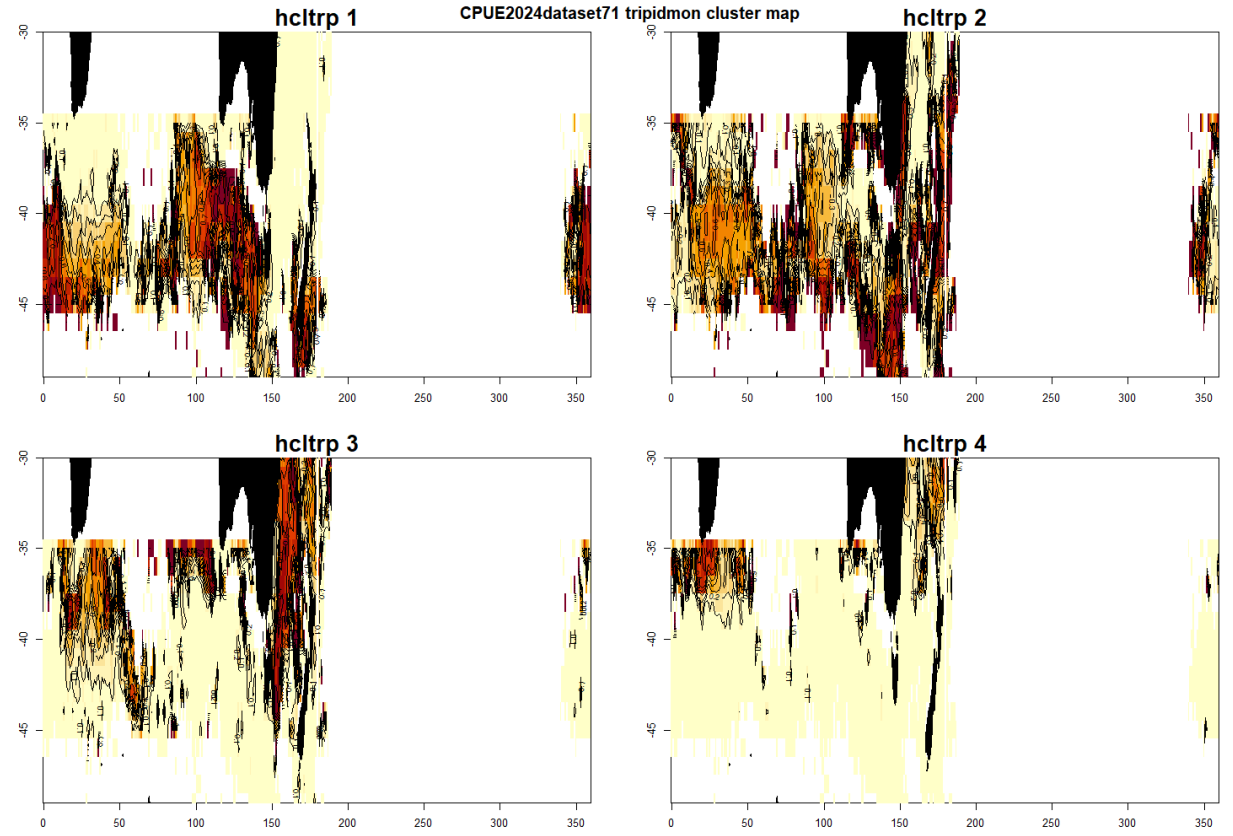

Fig. 8. Occurrence on map by group in the cluster analysis.

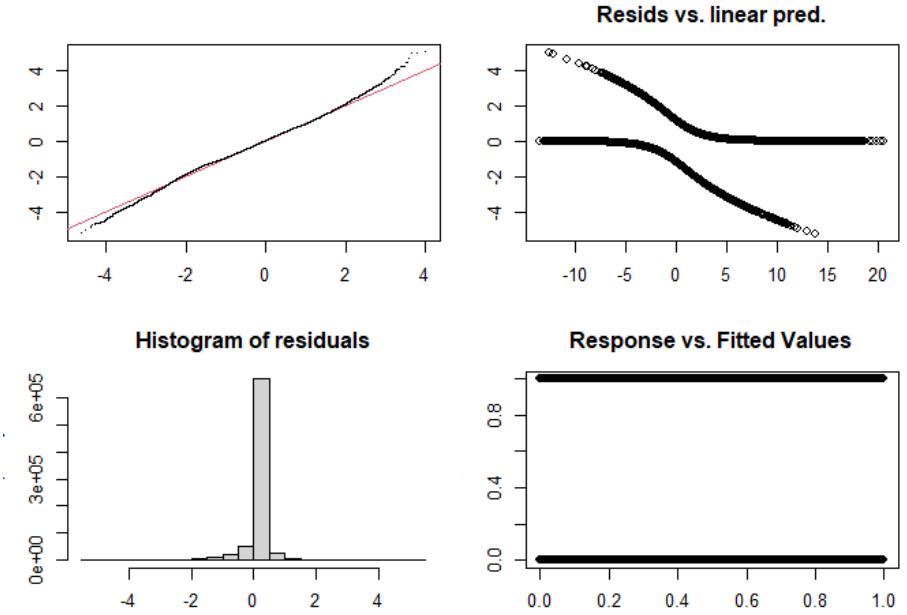

Fig. 9. Diagnostic plots for the binomial sub-model in the base case run.

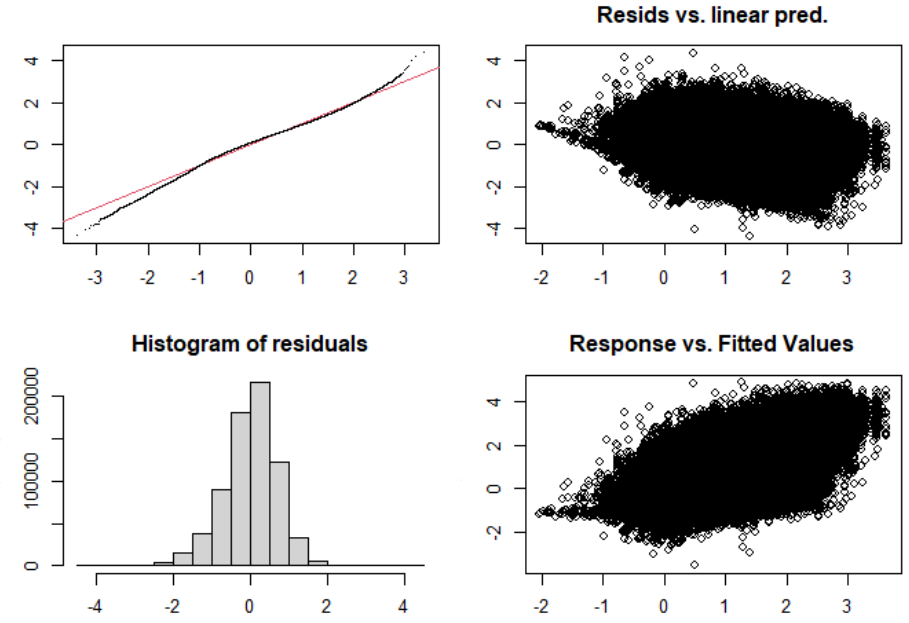

Fig. 10. Diagnostic plots for the positive catch sub-model in the base case run.

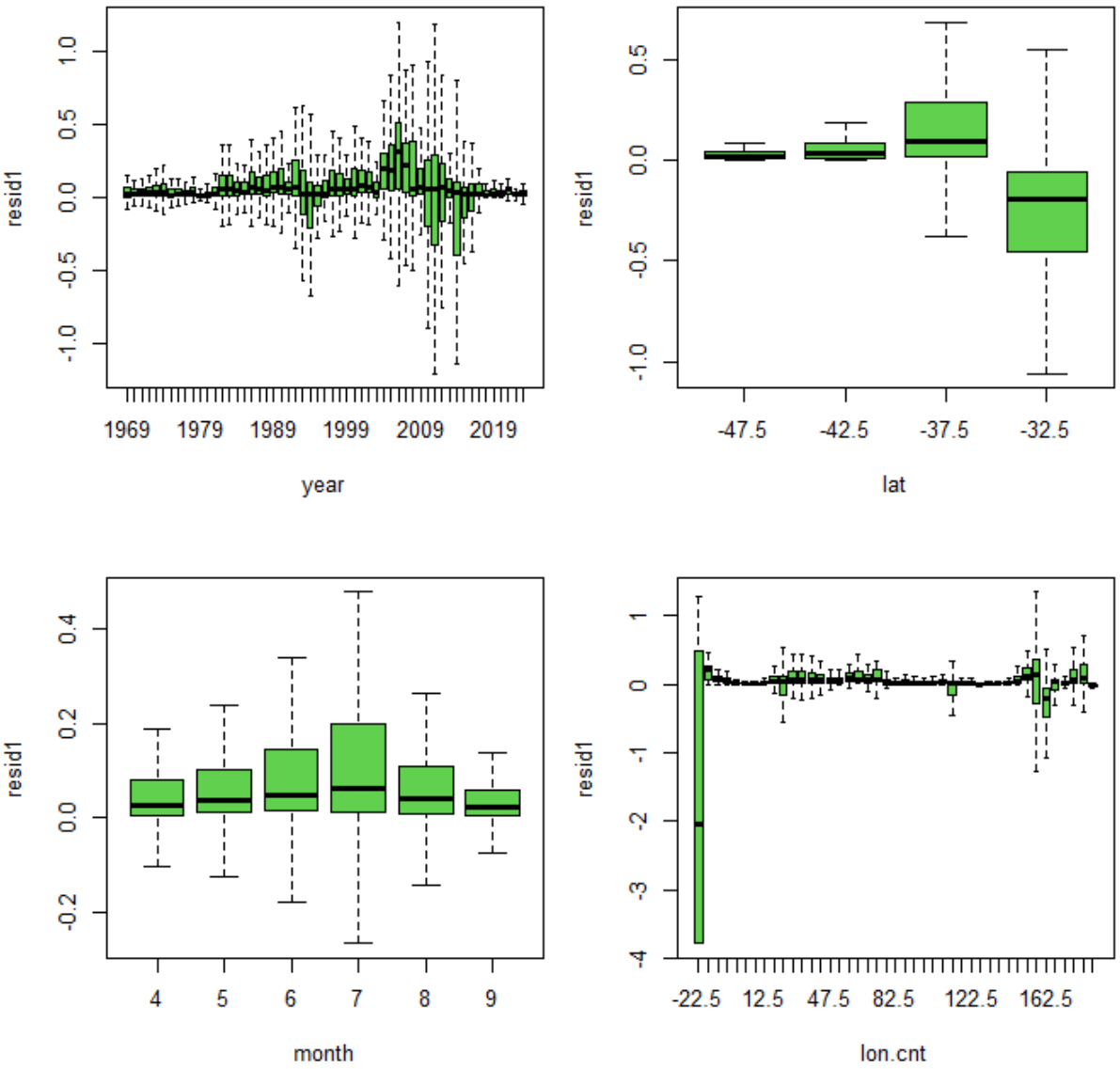

Fig. 11. Residuals by variable in the binomial sub-model in the base case run.

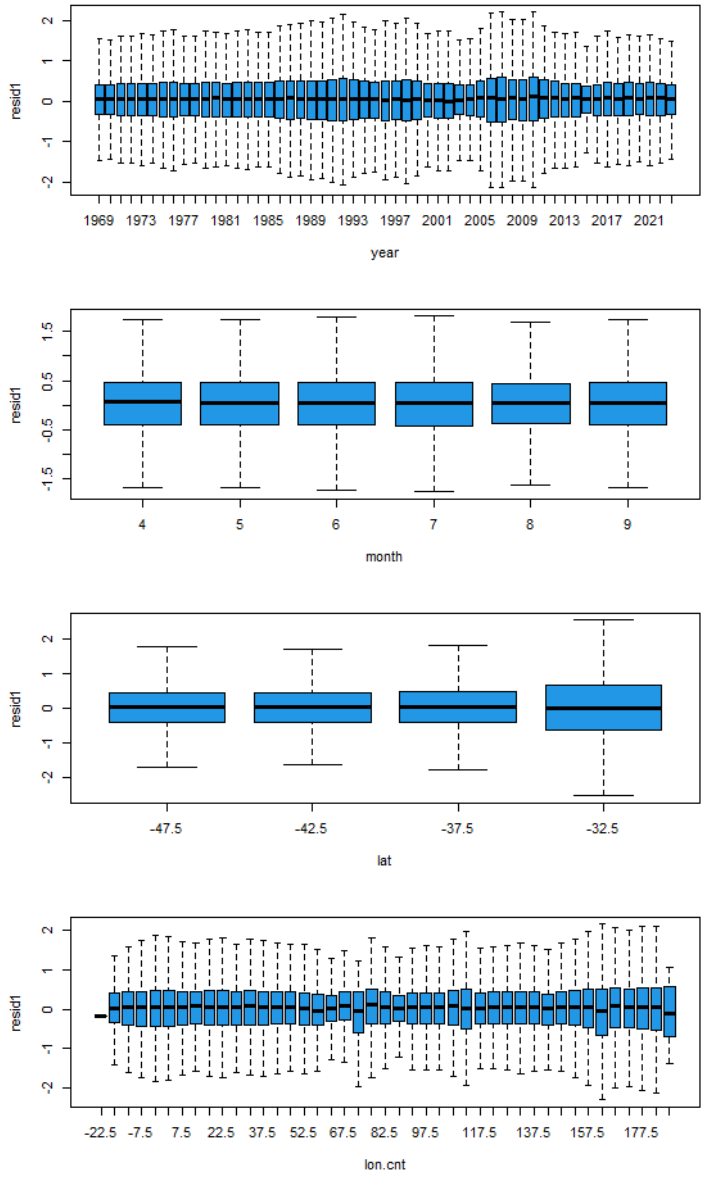

Fig. 12. Residuals by variable in the positive catch sub-model in the base case run.

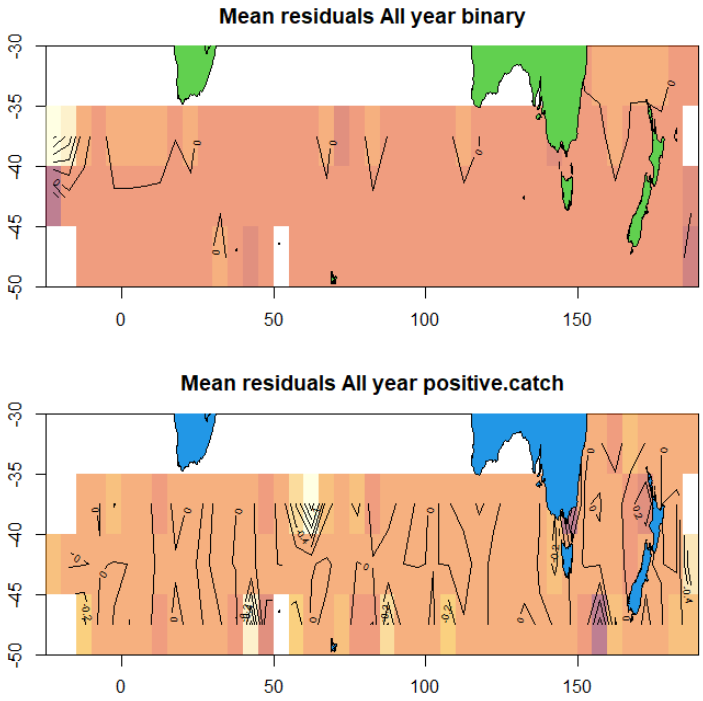

Fig. 13. Residual on maps for both sub-models in the base case run.

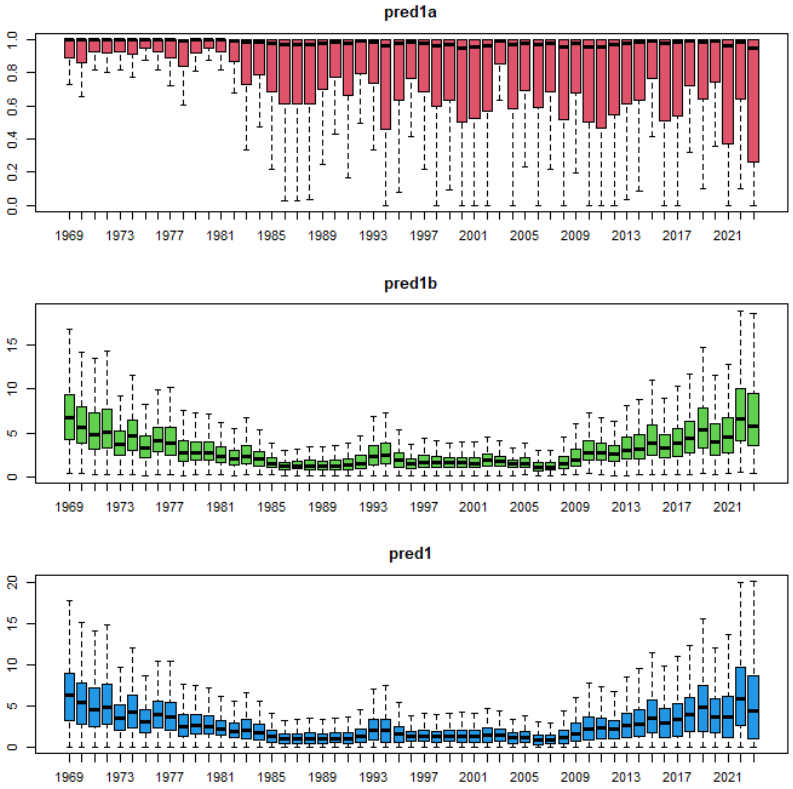

Fig. 14. Predicted value by year in the base case run.
Upper panel is the positive rate obtained from the binomial sub-model. Middle panels is CPUE obtained from the positive catch sub-model. Lower panel is product of the two.

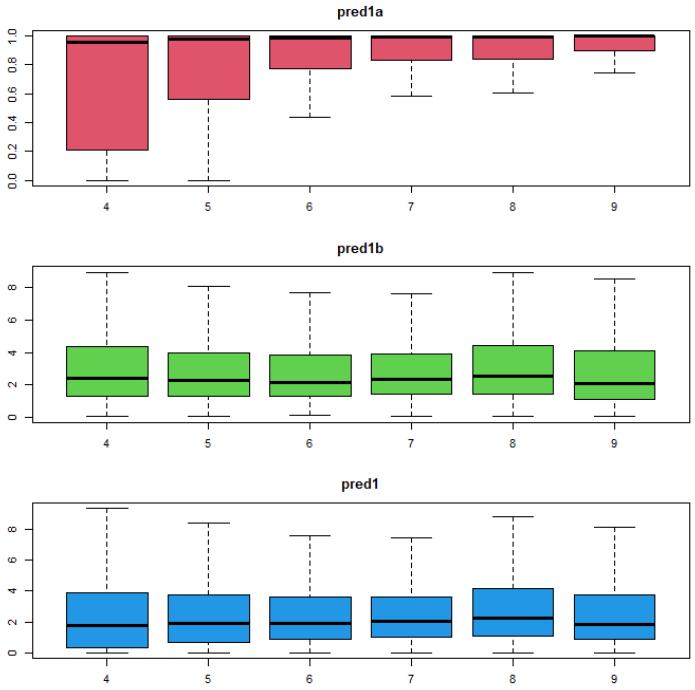

Fig. 15. Predicted value by month in the base case run.
See Fig. 14.

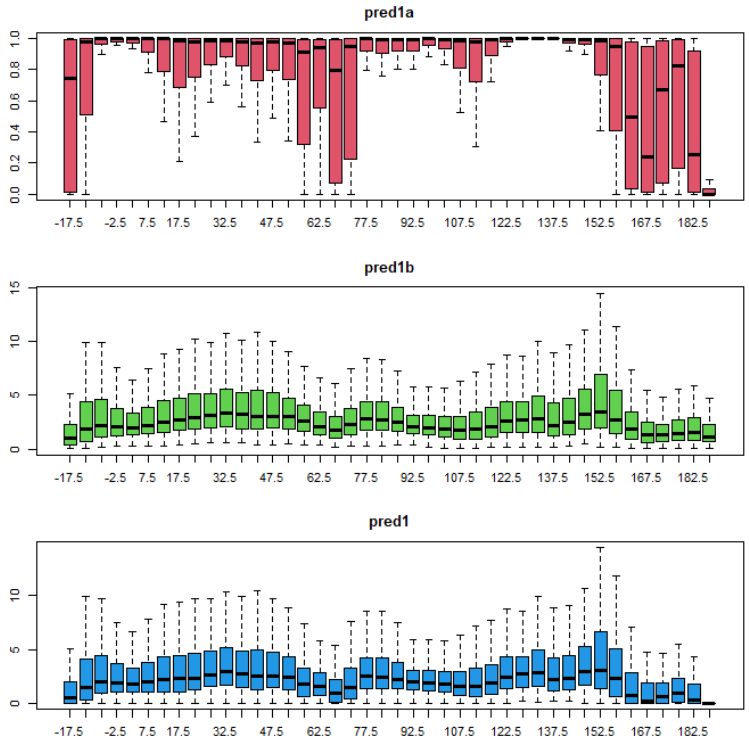

Fig. 16. Predicted value by longitude in the base case run.
See Fig. 14.

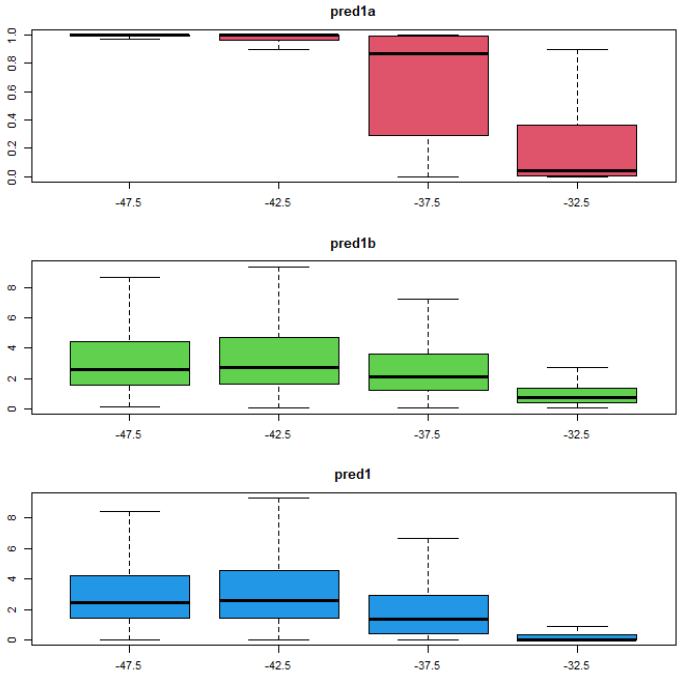

Fig. 17. Predicted value by latitude in the base case run.
See Fig. 14.

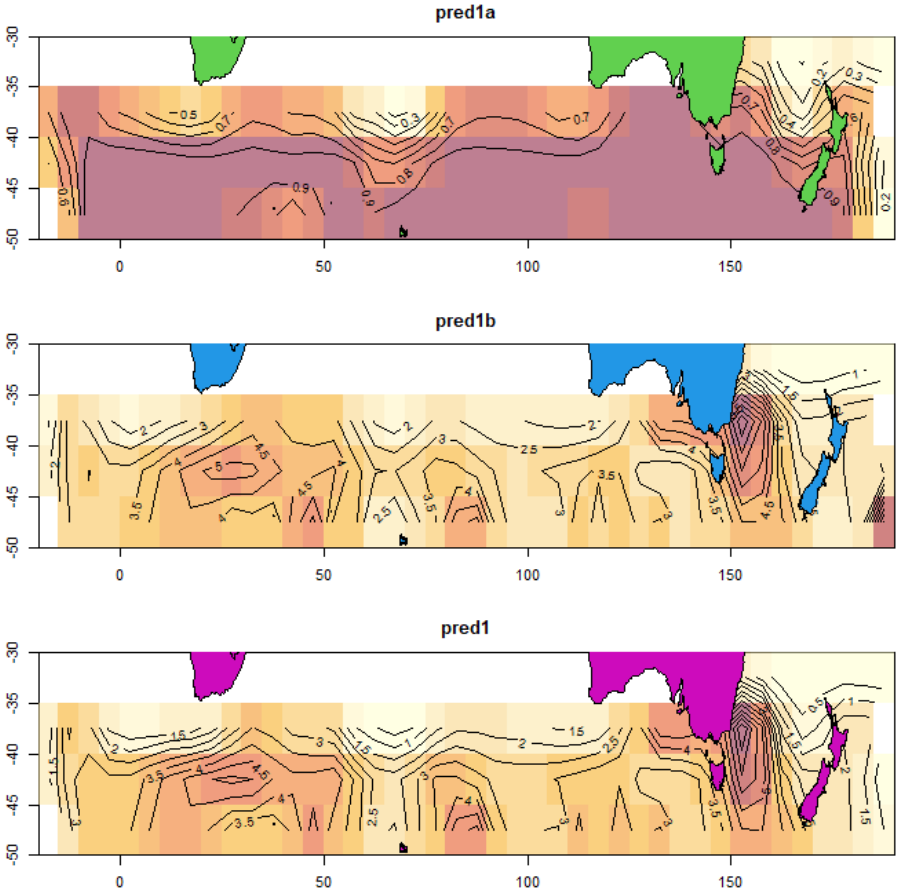

Fig. 18. Predicted value on map in the base case run.
See Fig. 14.

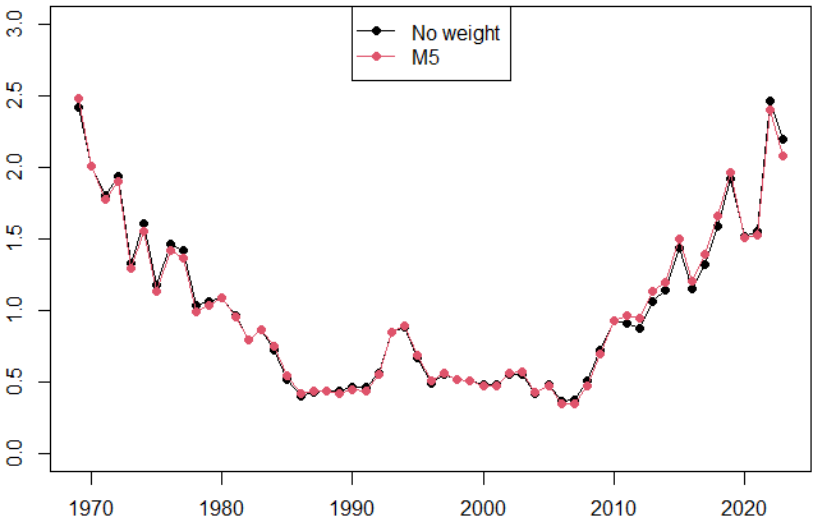

Fig. 19. Comparison of area weighted abundance indices in the base case run.
Red (M5) is area weighted abundance index which taking into account that the longitude length change over latitude and the number of 1x1 degree squares ever fished in a 5x5 degrees square. Black is the abundance index which weighting was not considered.

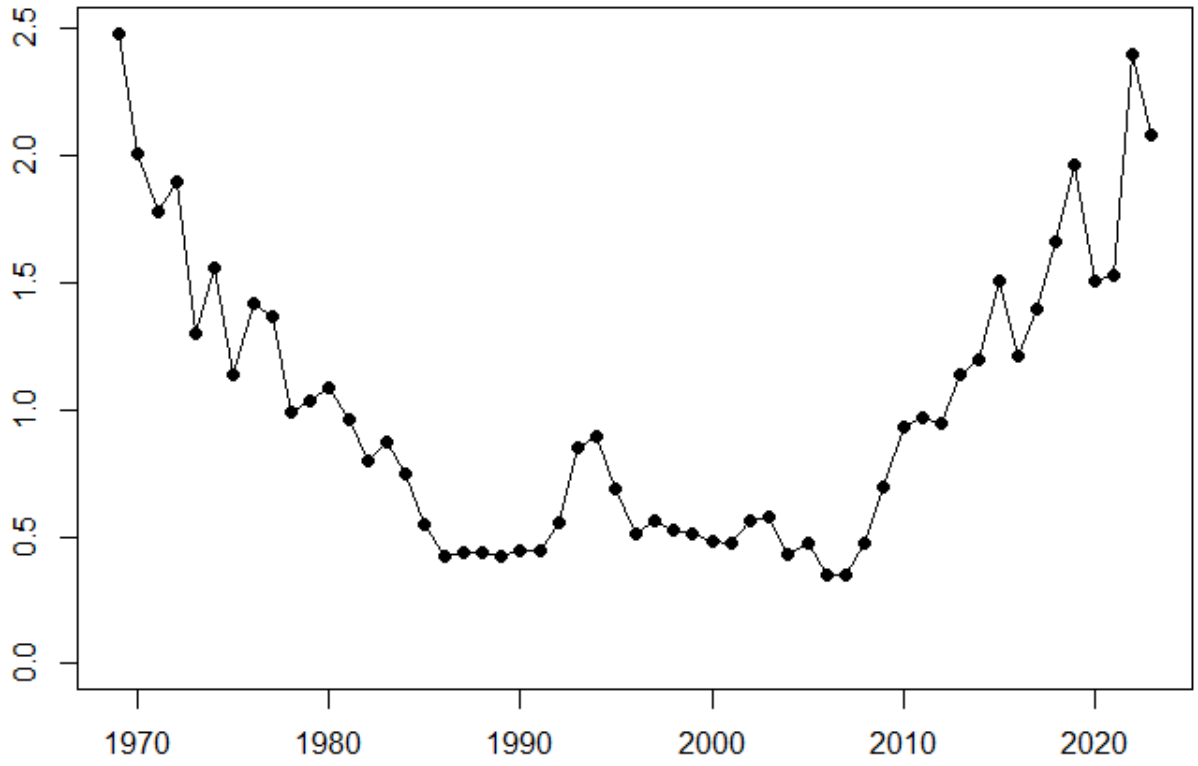

Fig. 20. CPUE abundance index for the base case.

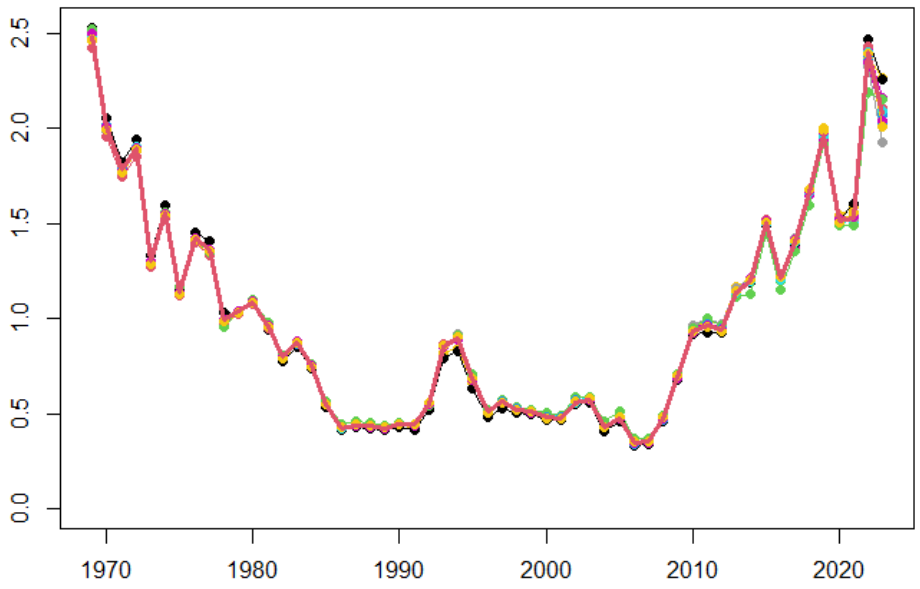

Fig. 21. Sensitivity analysis of model selection in the binomial sub-model for all runs.

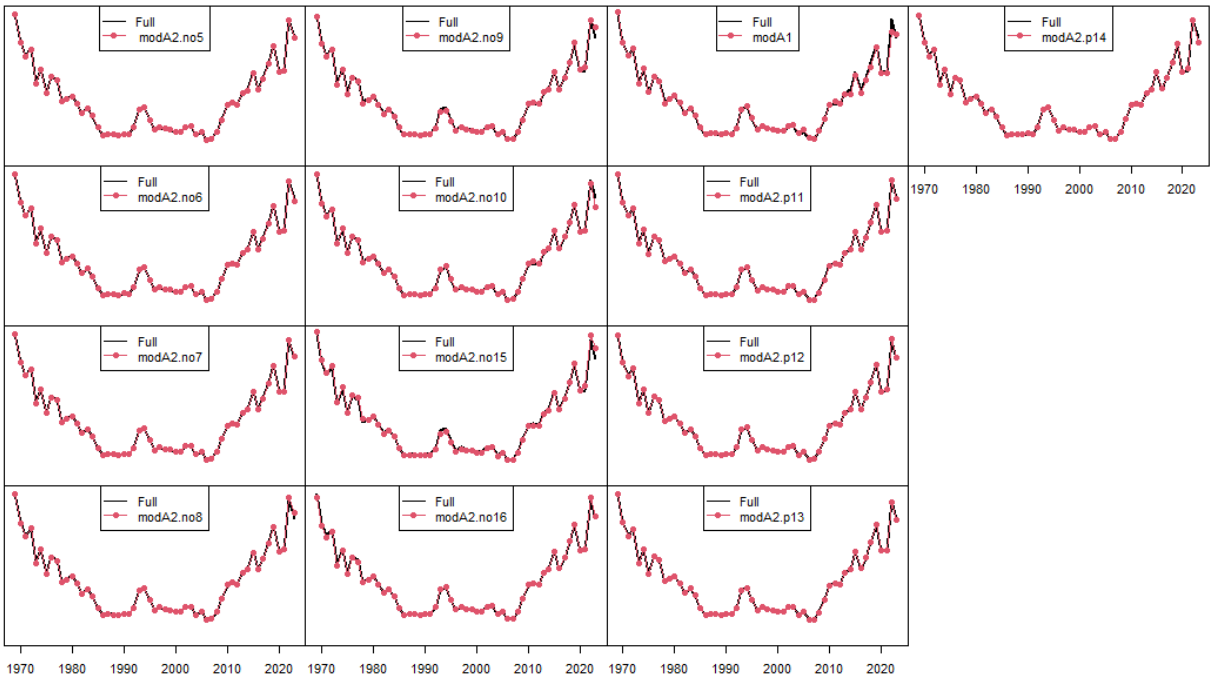

Fig. 22. Sensitivity analysis of model selection in the binomial sub-model for each run.
Full represents modA2.

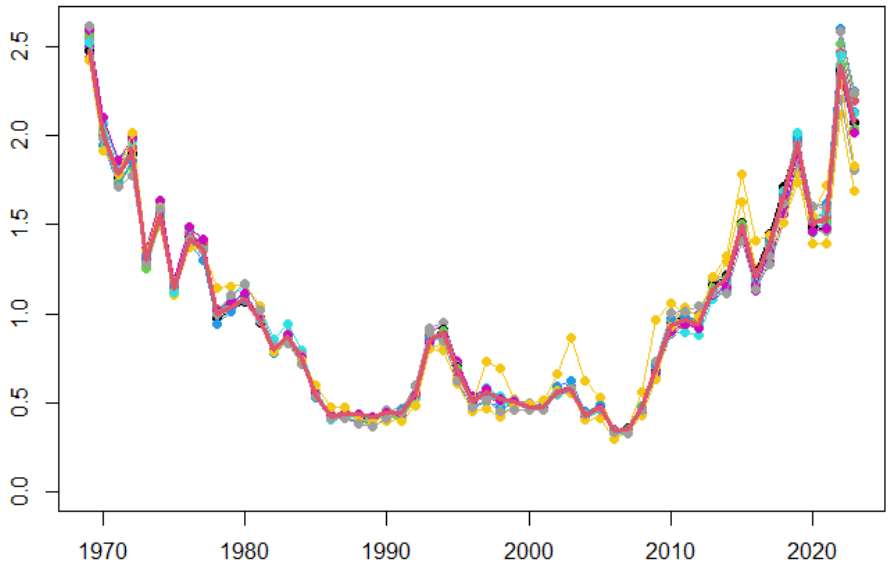

Fig. 23. Sensitivity analysis of model selection in the positive catch sub-model for all runs.

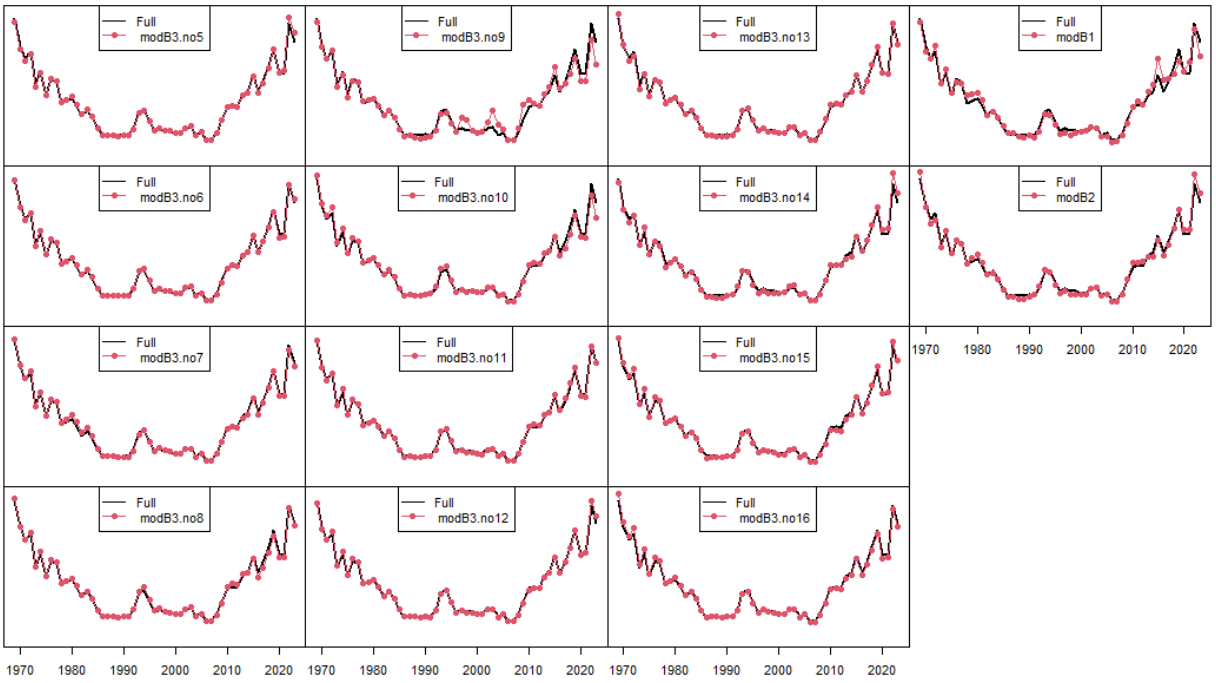

Fig. 24. Sensitivity analysis of model selection in the positive catch sub-model for each run.
Full represents modB3.

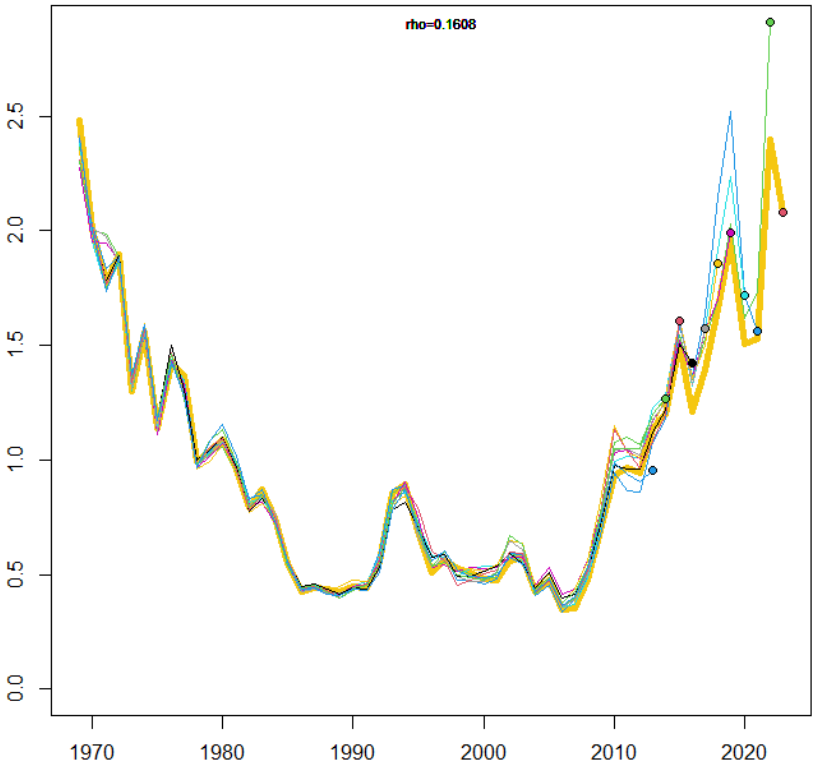

Fig. 25. Retrospective analysis for the base case model.
Rho represents Mohn's rho.

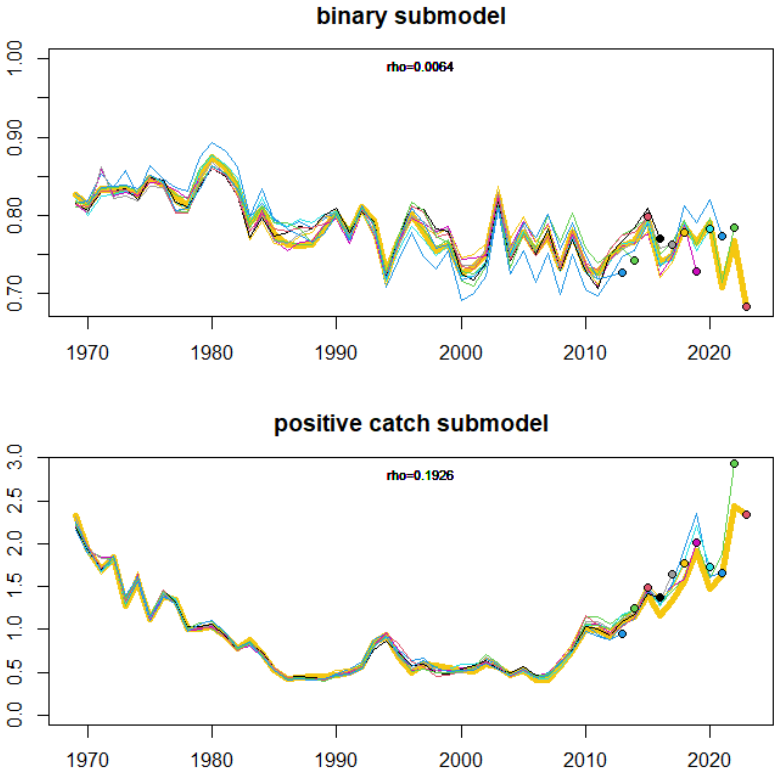

Fig. 26. Retrospective analysis for the base case model by sub-model.
Upper panel is by binomial submodel and lower panels is by positive catch submodel. Rho represents Mohn's rho.

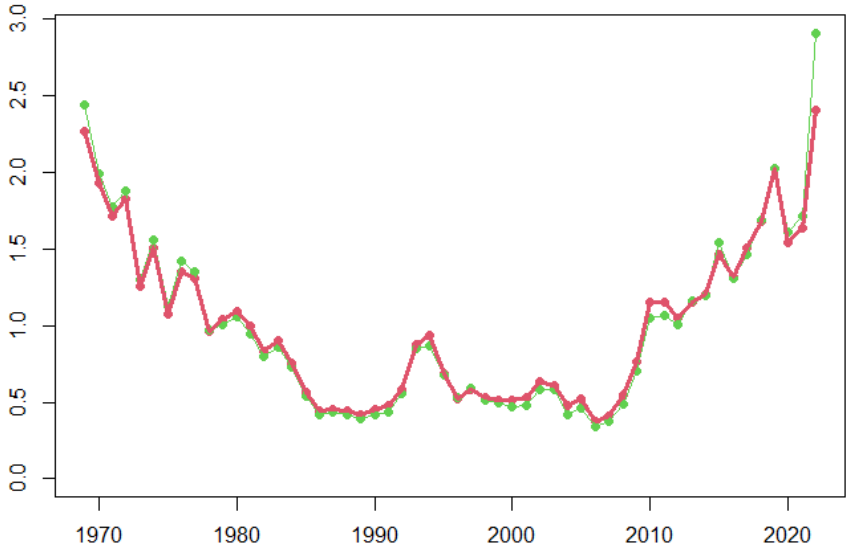

Fig. 27. Two indices from datasets up to 2022 by the datasets made in 2023 (red) and 2024 (green).

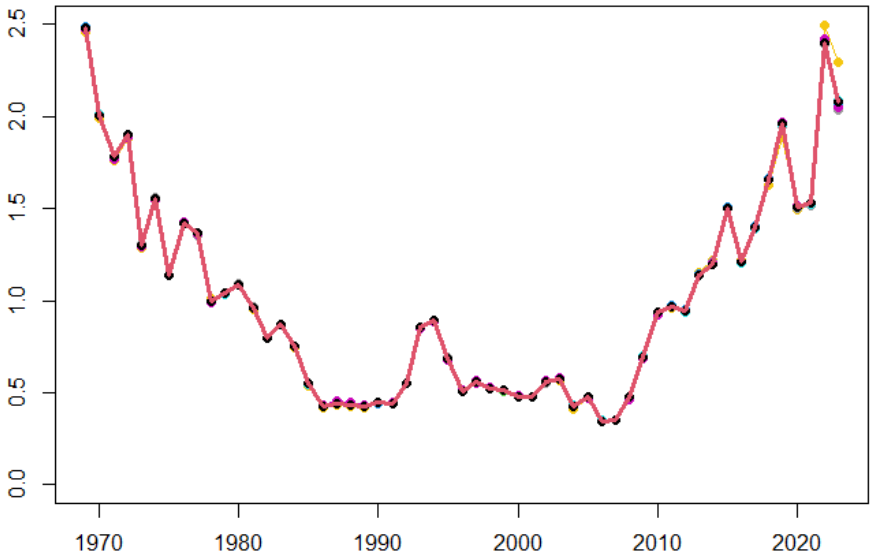

Fig. 28. Sensitivity analysis of k-value in the binomial sub-model for all runs.

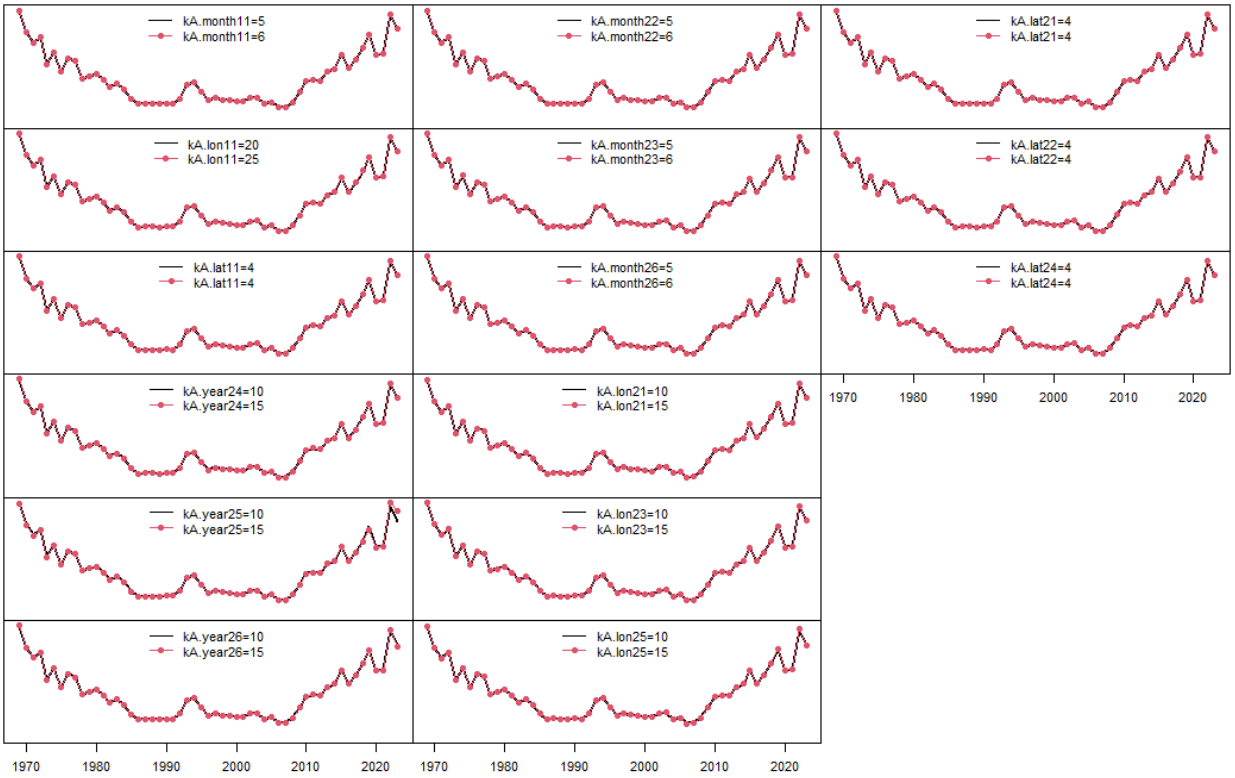

Fig. 29. Sensitivity analysis of k-value in the binomial sub-model for each of run.

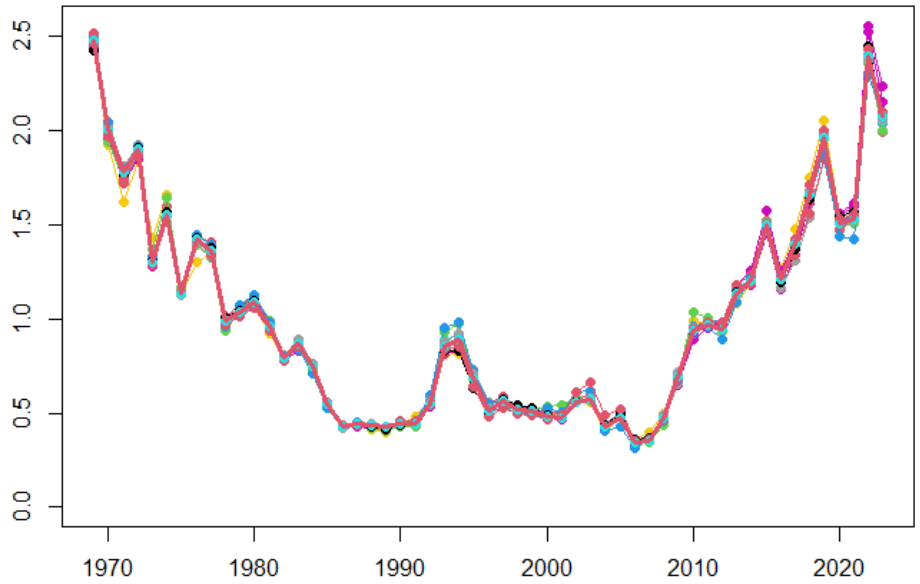

Fig. 30. Sensitivity analysis of k-value in the positive catch sub-model for all runs.

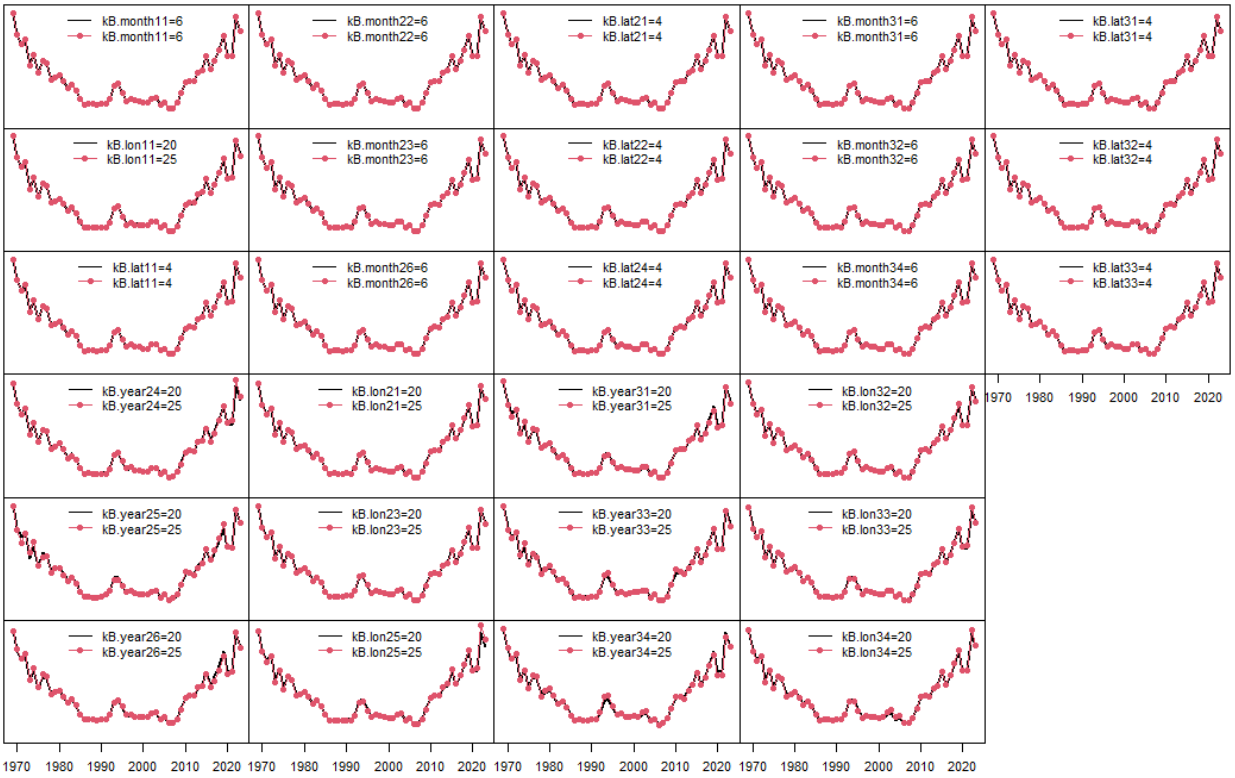

Fig. 31. Sensitivity analysis of k-value in the positive catch sub-model for each of run.

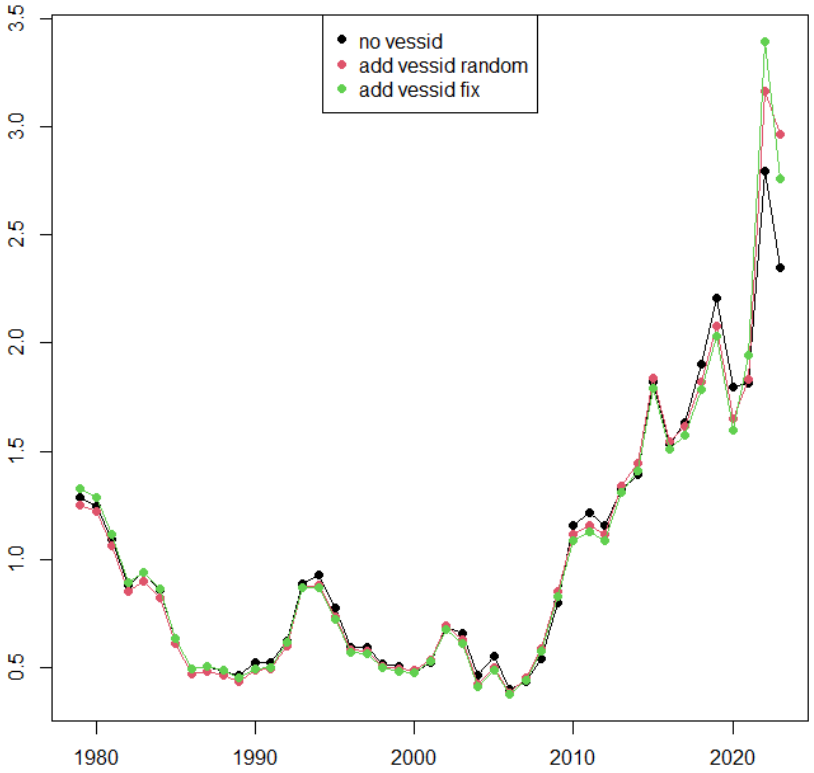

Fig. 32. Sensitivity analysis for the effect of vessel ID.

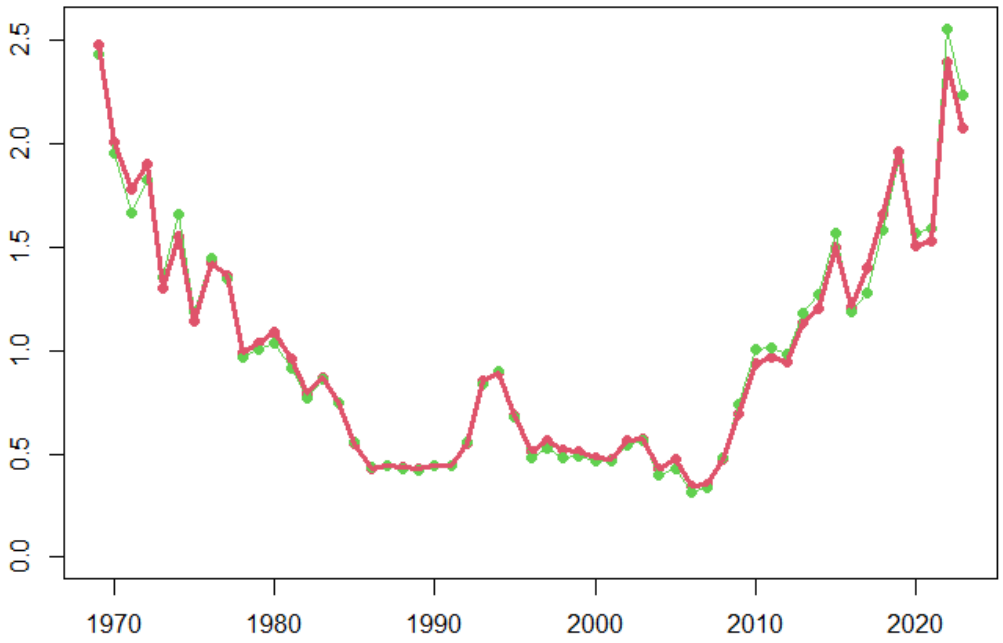

Fig. 33. Sensitivity analysis for the effect of eliminating 30S from the data.
Red is the base case, and green is the sensitivity run (eliminate 30S).

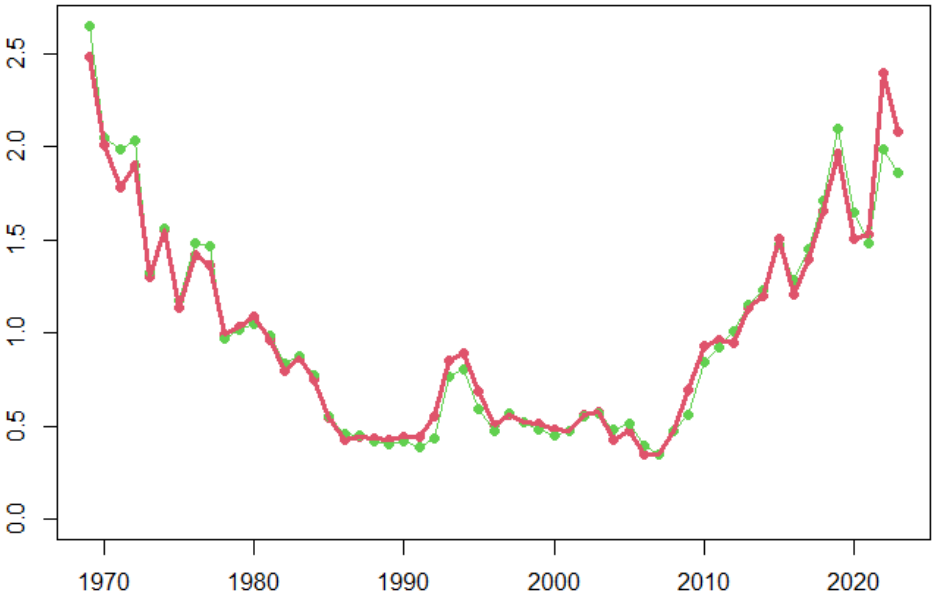

Fig. 34. Sensitivity analysis for the effect of age-5 plus instead of age-4 plus.
Red is the base case, and green is the sensitivity run (age-5 plus).

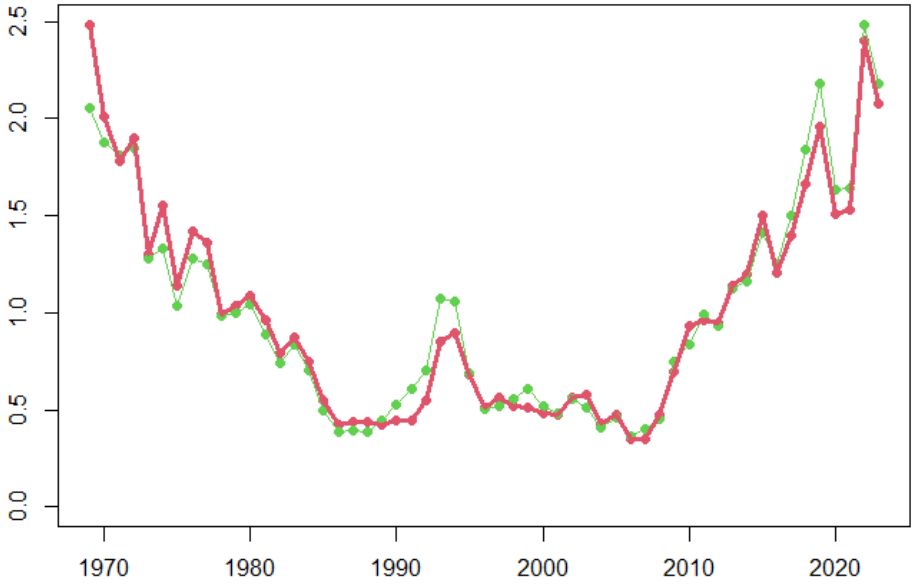

Fig. 35. Sensitivity analysis for the effect of of all ages instead of age-4 plus.
Red is the base case, and green is the sensitivity run (all ages).

Fig. 36. Sensitivity analysis for the effect of data resolution in 5 degree.
Red is the base case, and green is the sensitivity run (aggregated by month and 5 degree latitude and 5 degree longitude).

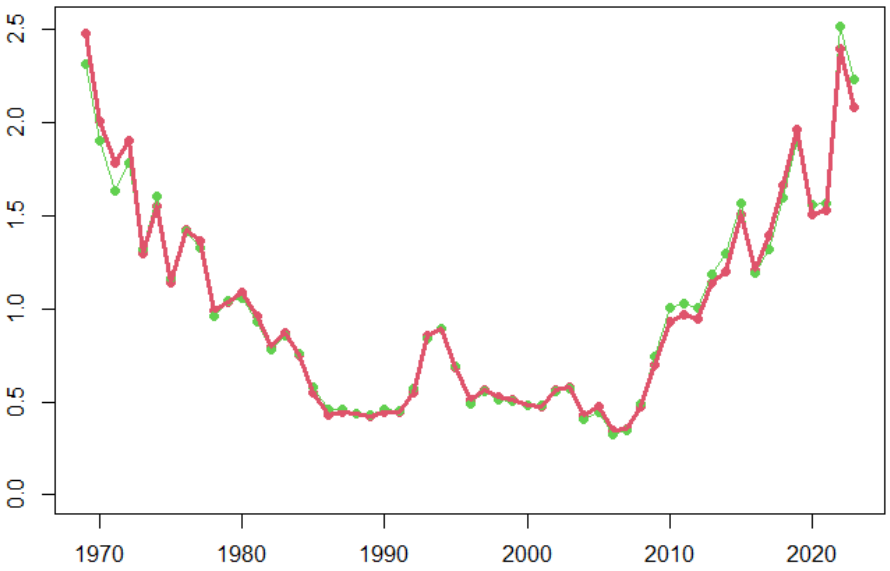

Fig. 37. Sensitivity analysis for the effect of data resolution in 1 degree.
Red is the base case, and green is the sensitivity run (aggregated by month and 1 degree latitude and 1 degree longitude).

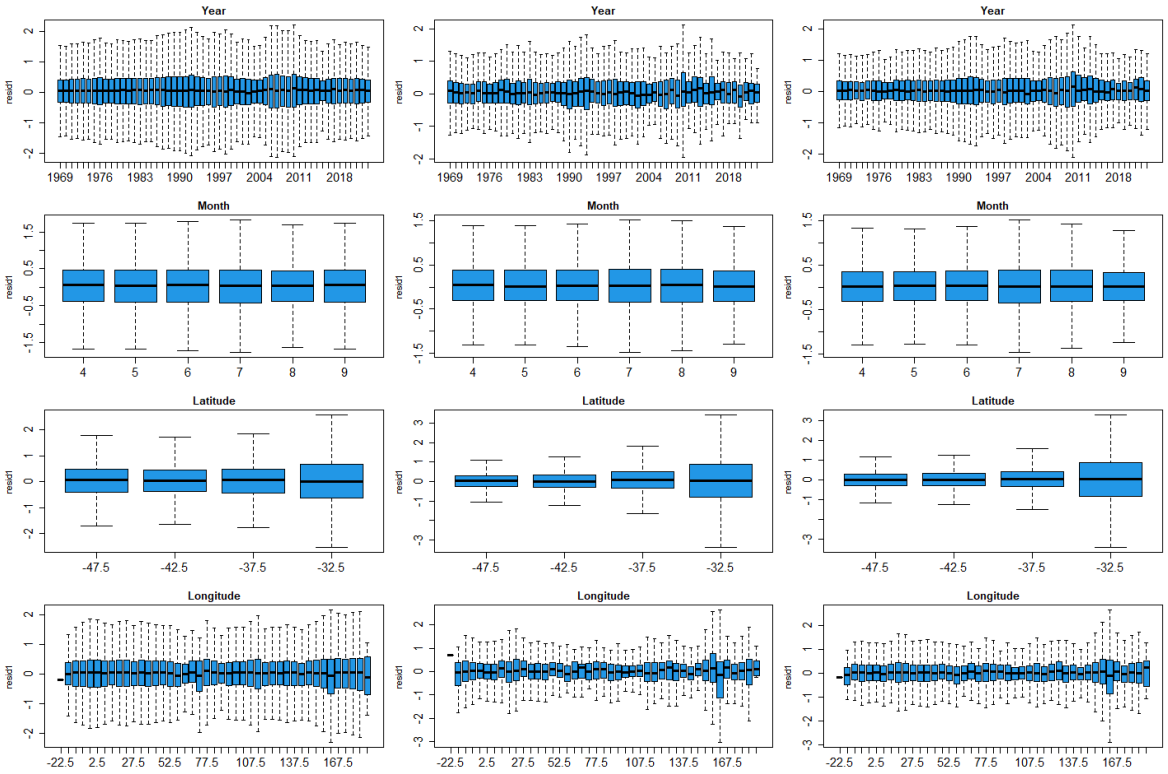

Fig. 38. Sensitivity analysis for the effect of data aggregation by residuals in the positive catch sub-model.
Left is shot-by-shot data, middle is 5 degree data and right is 1 degree data.

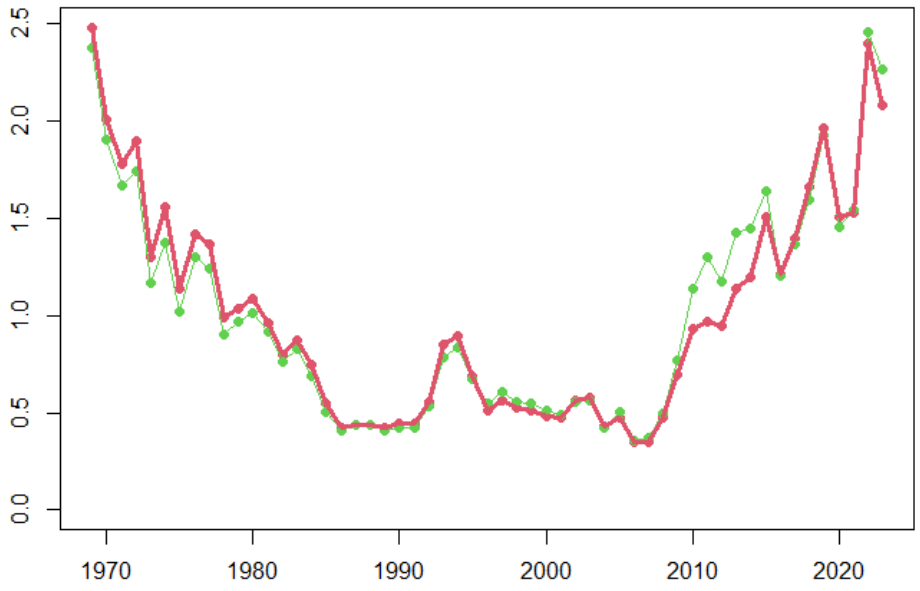

Fig. 39. Sensitivity analysis for the effect of resolution in model.
Red is the base case, where 5 degree for latitude and longitude, and green is the sensitivity run (1 degree in the model).

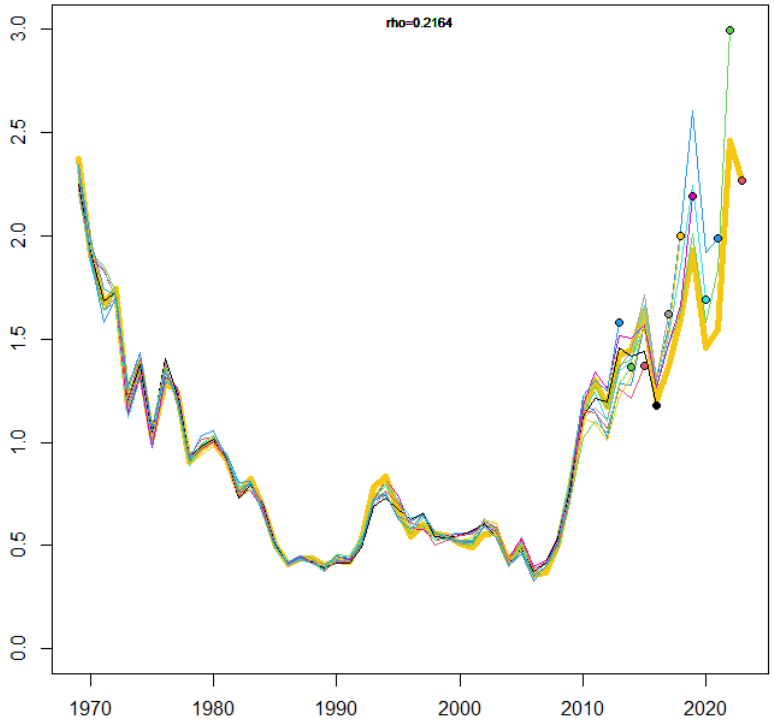

Fig. 40. Retrospective analysis in the sensitivity analysis of 1 degree model.

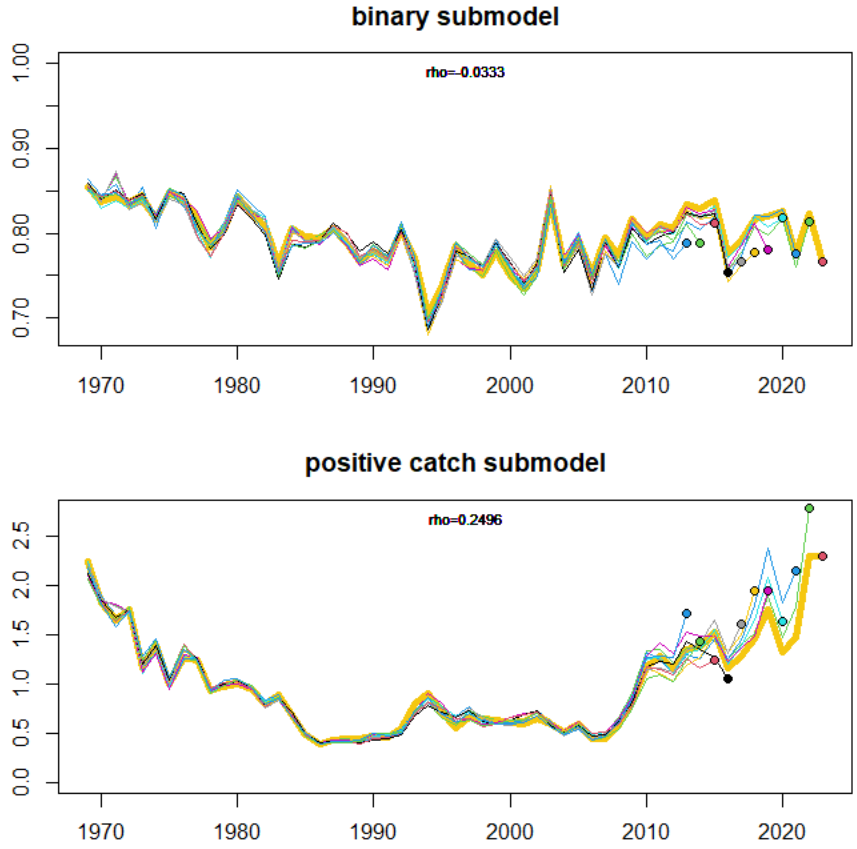

Fig. 41. Retrospective analysis in the sensitivity analysis of 1 degree model by sub-model.
Upper panel is by binomial submodel and lower panels is by positive catch submodel.

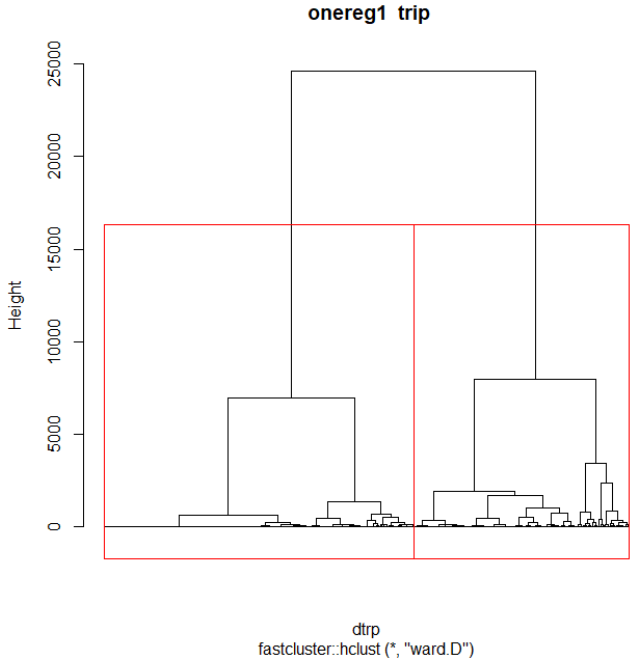

Fig. 42. Dendrogram in the cluster analysis of sensitivity analysis for the effect of 2 clusters.

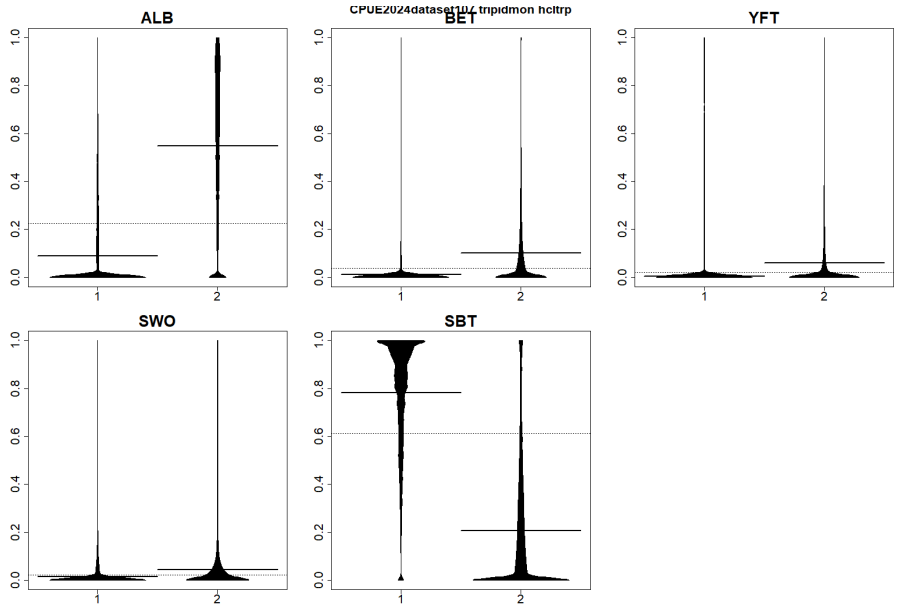

Fig. 43. Occurrence by species in the group in the 2 cluster analysis as a sensitivity analysis.

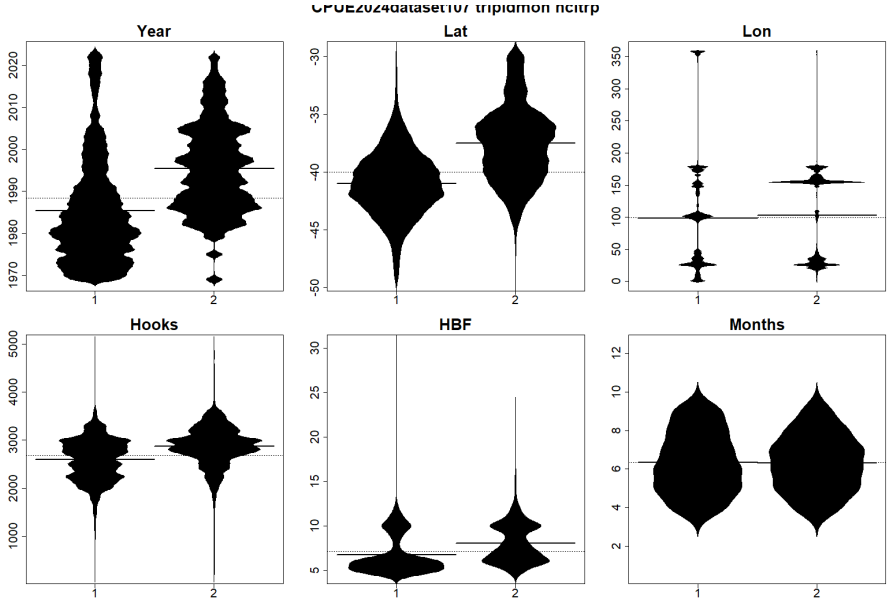

Fig. 44. Occurrence by variables in the group in the 2 cluster analysis as a sensitivity analysis.

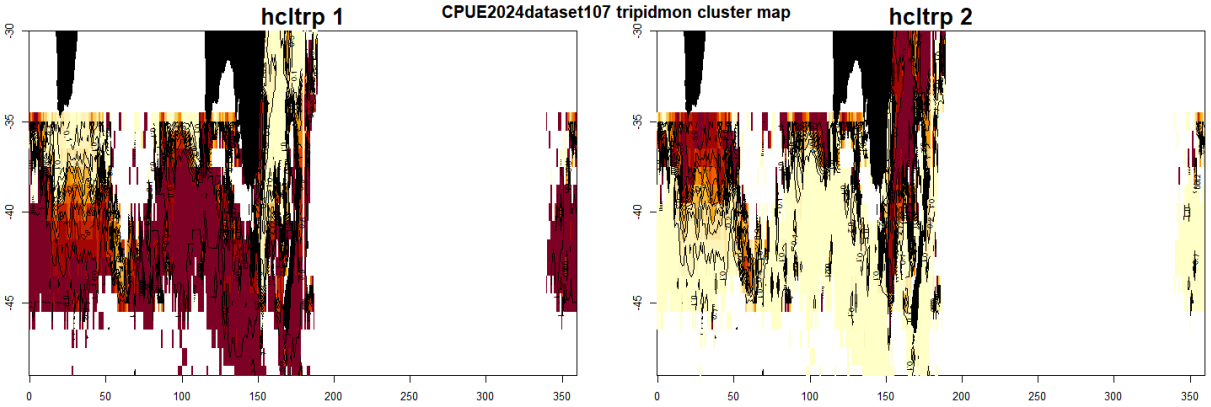

Fig. 45. Occurrence on map in the group in the 2 cluster analysis as a sensitivity analysis.

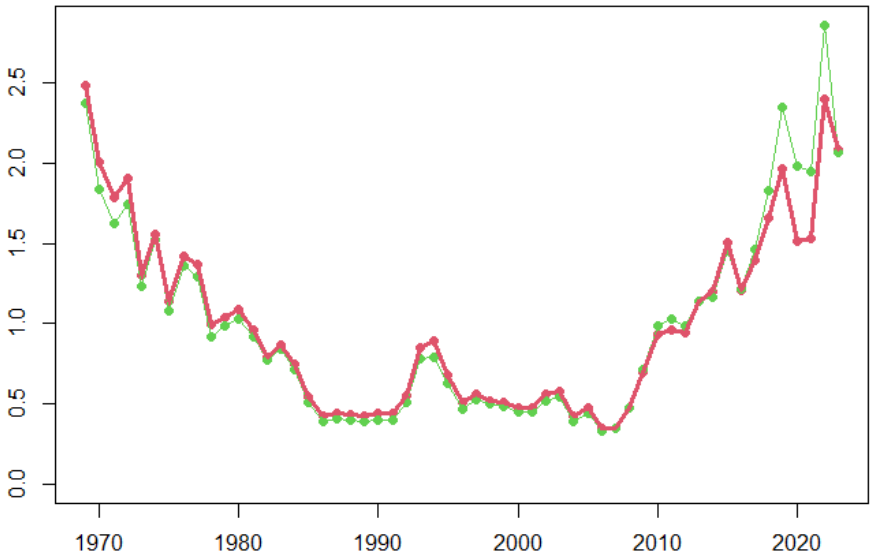

Fig. 46. Sensitivity analysis for the effect of 2 clusters instead of 4 clusters in the abundance index.
Red is the base case, and green is the sensitivity run (2 clusters).

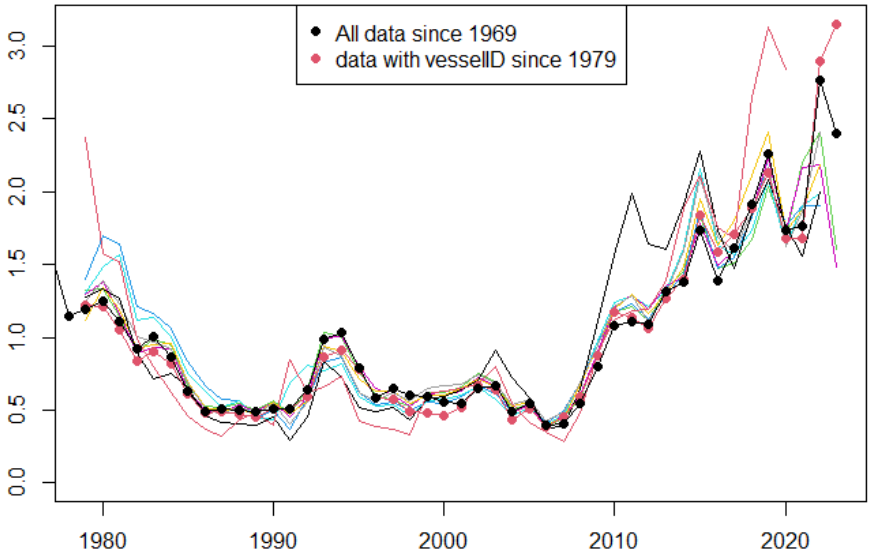

Fig. 47. Sensitivity analysis of core vessels selection.
Black and red lines with dots are the index from all vessels since 1969 and 1979, respectively. Black line is adjusted to the mean since 1979. Indices from different core vessels data are shown in different colors.

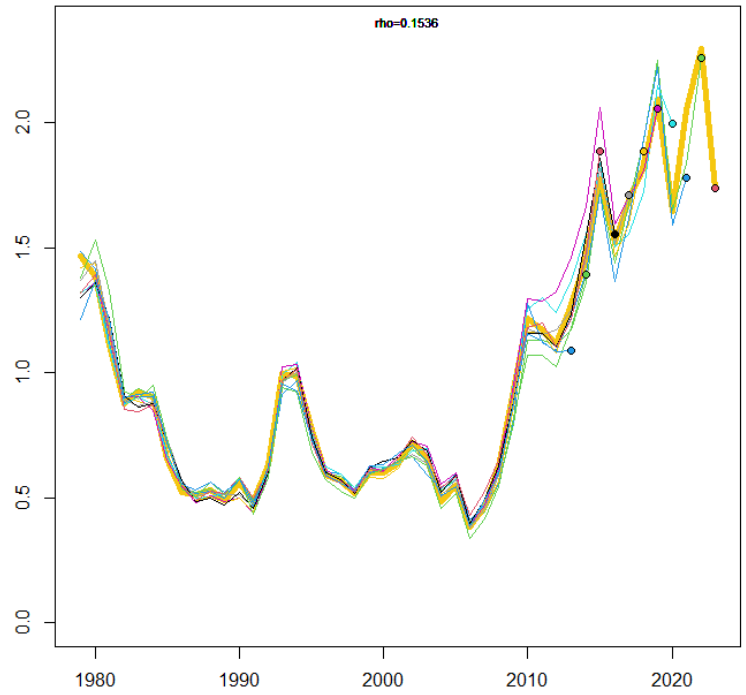

Fig. 48. Retrospective analysis in the sensitivity analysis of the core vessel.
rho is Mohn's rho value.

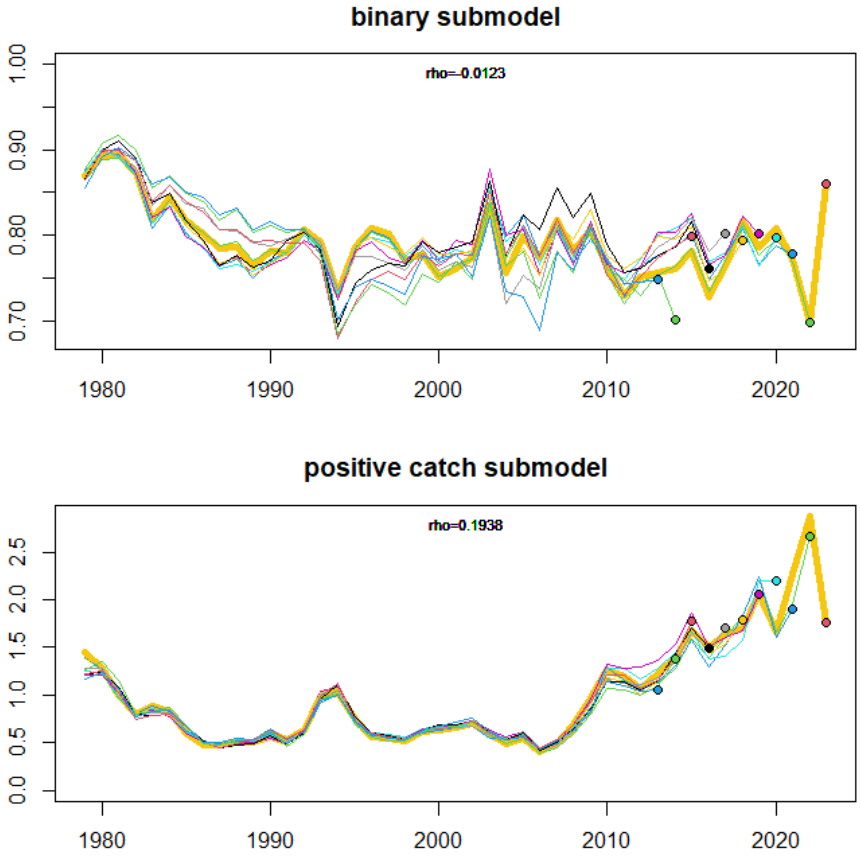

Fig. 49. Retrospective analysis in the sensitivity analysis of the core vessel by sub-model.
Upper panel is by binomial submodel and lower panels is by positive catch submodel. rho is Mohn's rho value..

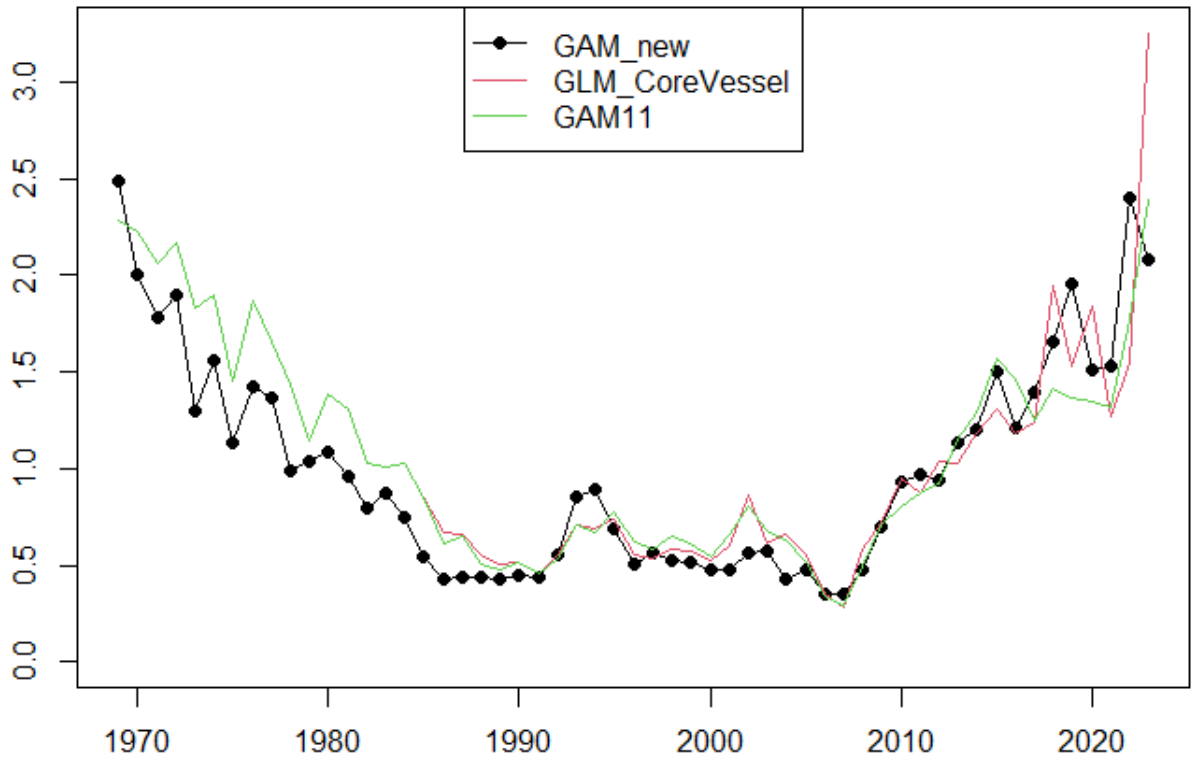

Fig. 50. Comparison of three abundance indices.
GLM_CoreVessel is the index by core vessel data with GLM base model in W0.8. GAM11 is the GAM model W0.8 used for the stock assessment in 2020.

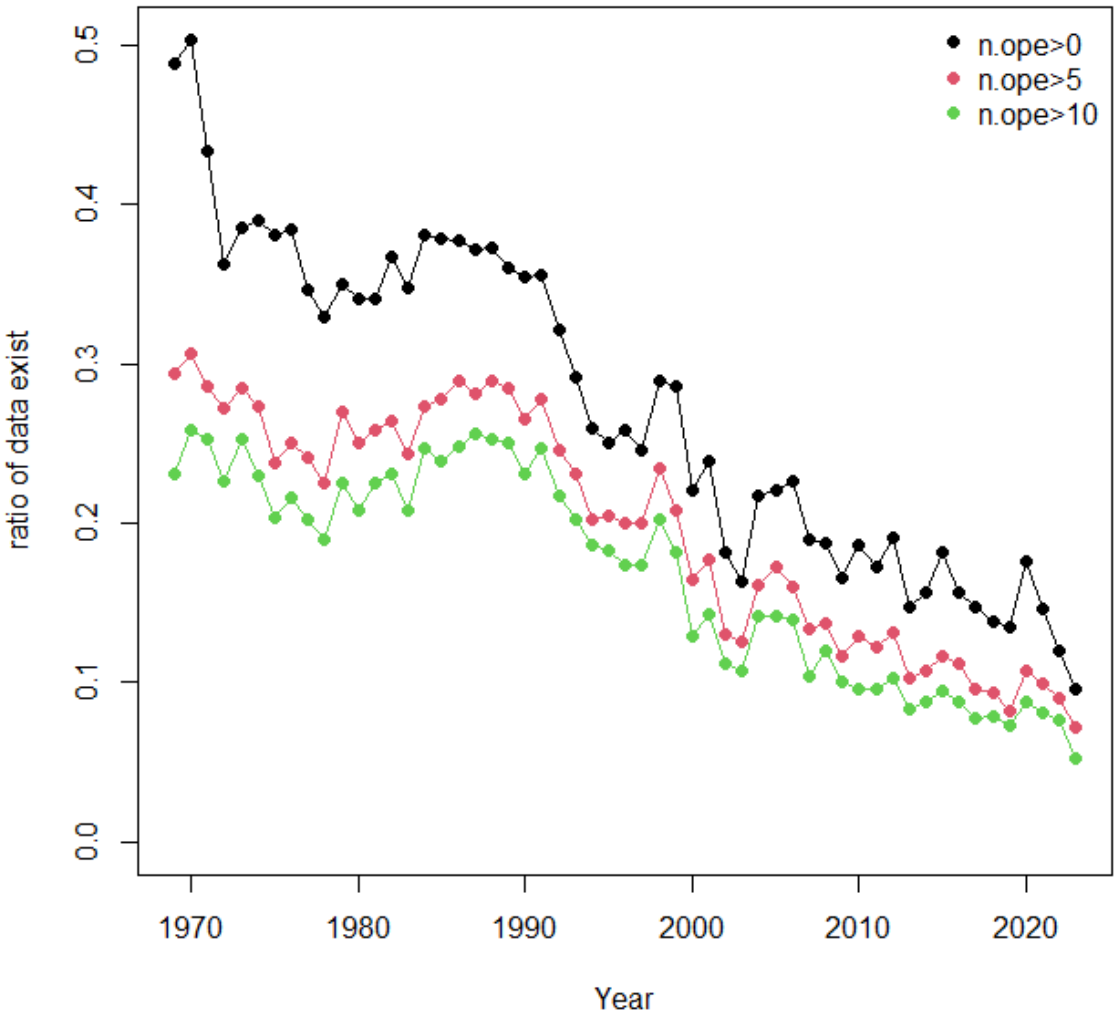

Fig. 51. Proportion of actual data existed in the dummy data used for glm/gam prediction by year.
The number of operations >0, >5 and >10 are shown in black, red and green, respectively.

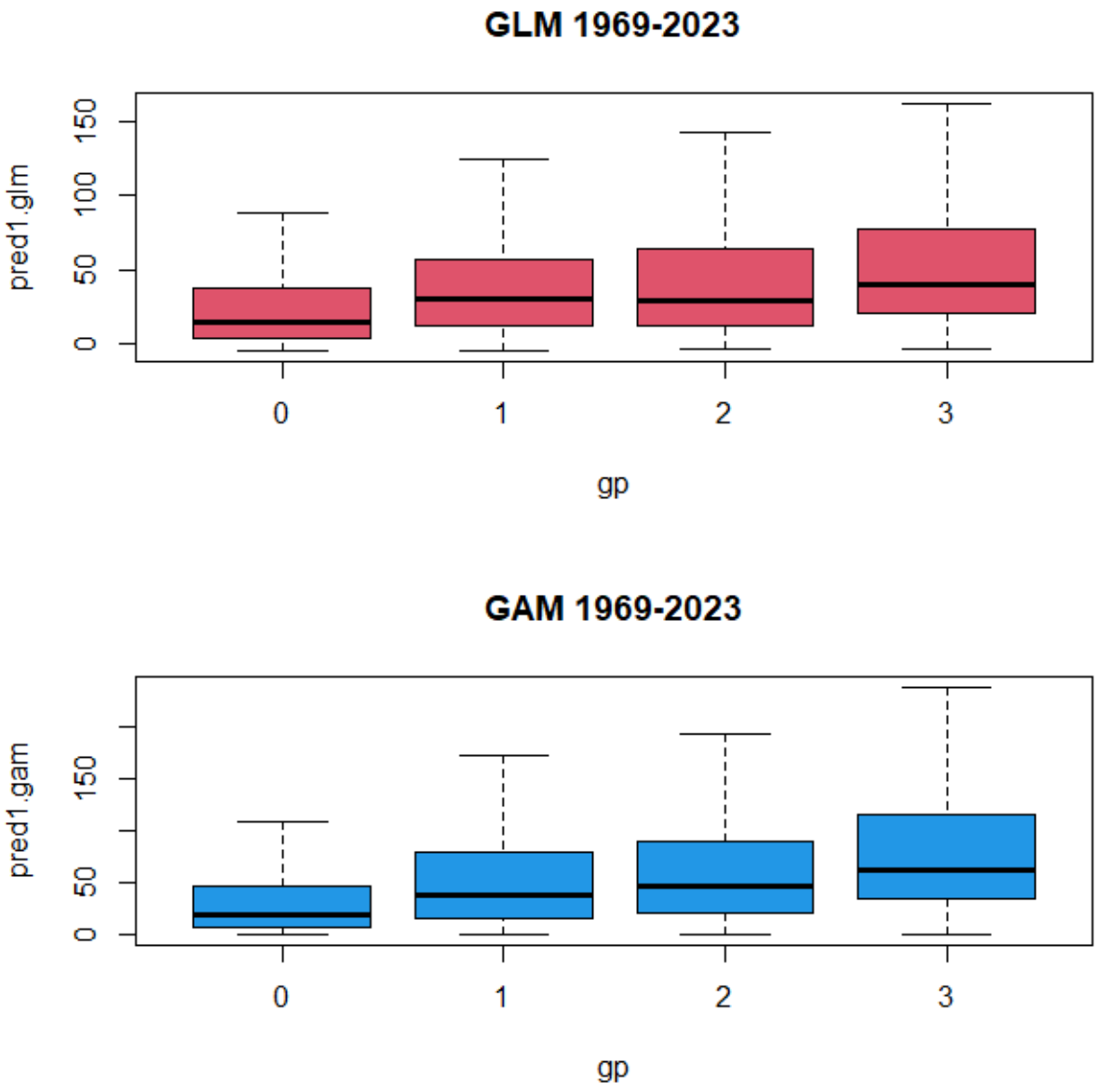

Fig. 52. Boxplot of CPUE predicted values by category group without outliers.
Group 0 is the number of operation in actual data corresponded was 0. Group 1 is >=1 and < 5 operations. Group 2 is >=5 and < 10 operations and Group 3 is > 10 operations. Data in all years were combined.

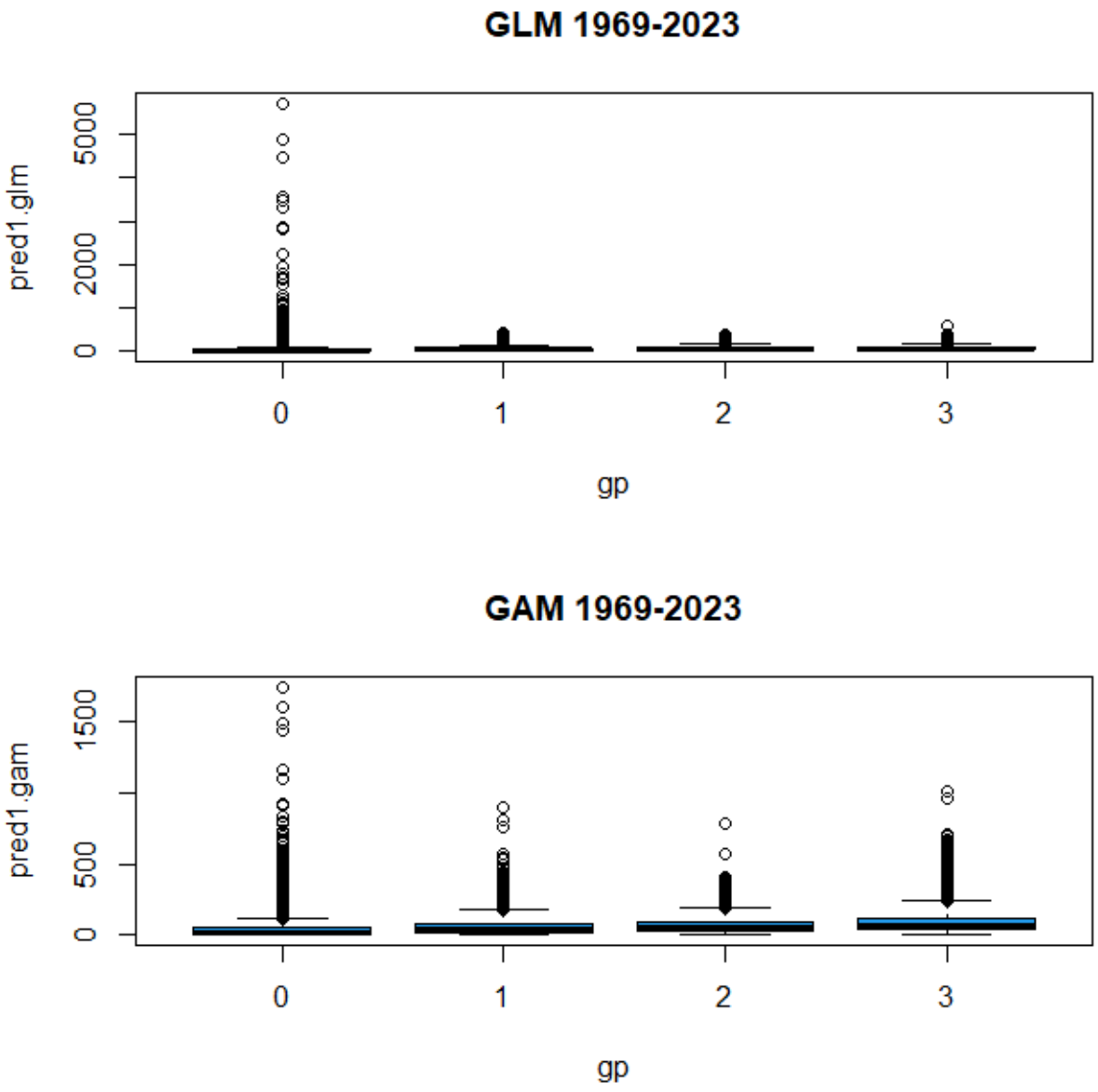

Fig. 53. Boxplot of CPUE predicted values by category group with outliers.
Group 0 is the number of operation in actual data corresponded was 0. Group 1 is >=1 and < 5 operations. Group 2 is >=5 and < 10 operations and Group 3 is > 10 operations. Data in all years were combined.

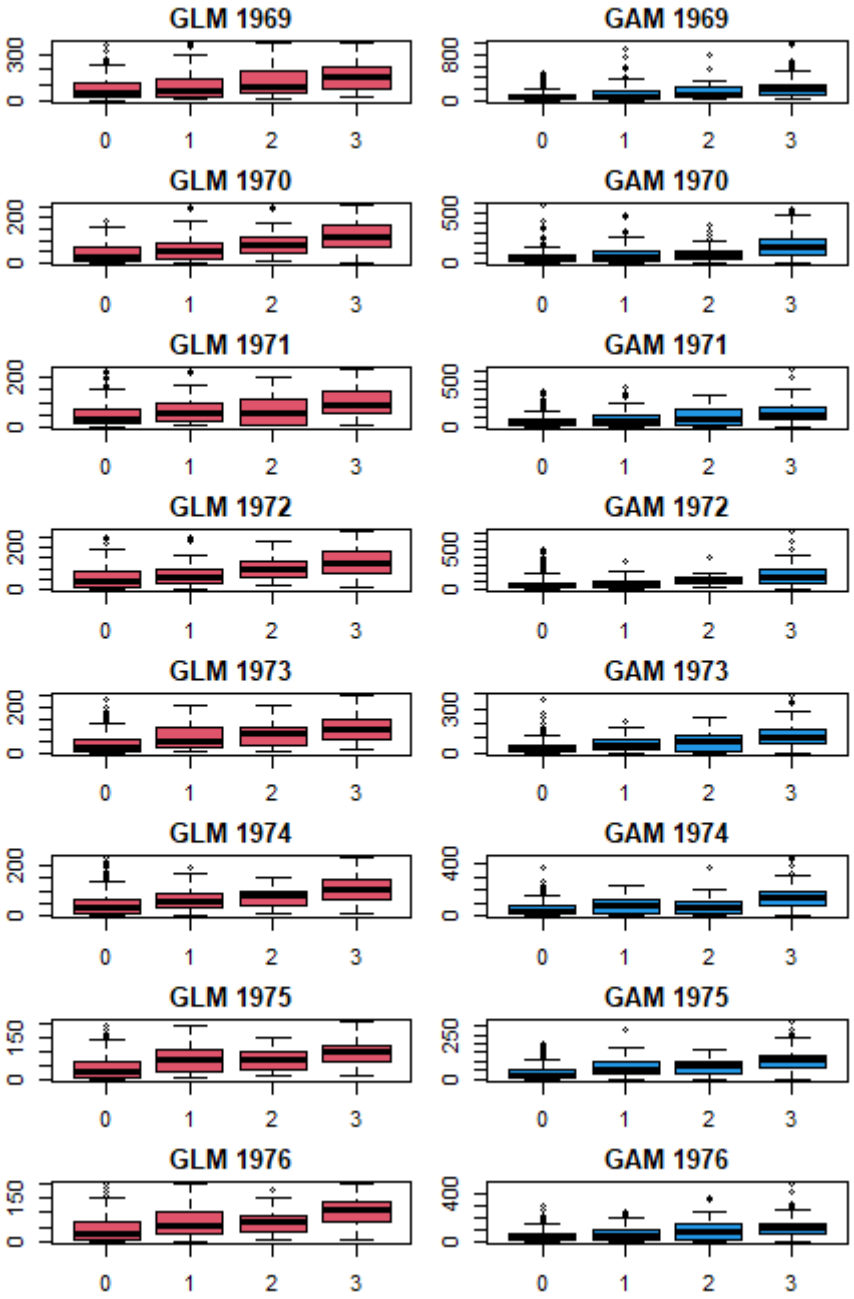

Fig. 54. Boxplot of CPUE predicted values by category group and year with outliers.
Group 0 is the number of operation in actual data corresponded was 0. Group 1 is >=1 and < 5 operations. Group 2 is >=5 and < 10 operations and Group 3 is > 10 operations.

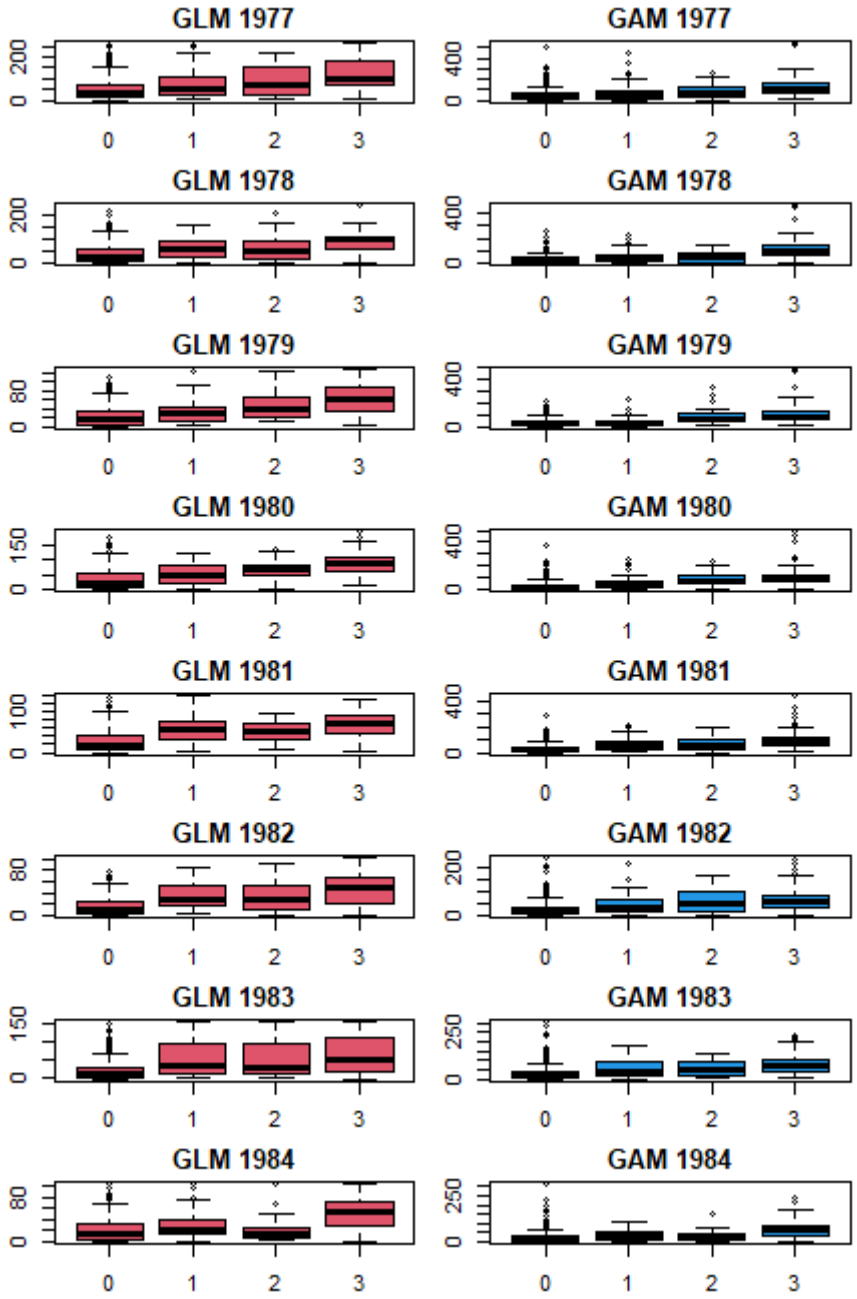
GLM 1977
GAM 1977
GLM 1978
GAM 1978
GLM 1979
GAM 1979
GLM 1980
GAM 1980
GLM 1981
GAM 1981
GLM 1982
GAM 1982
GLM 1983
GAM 1983
GLM 1984
GAM 1984

Fig. 54. (Cont'd)

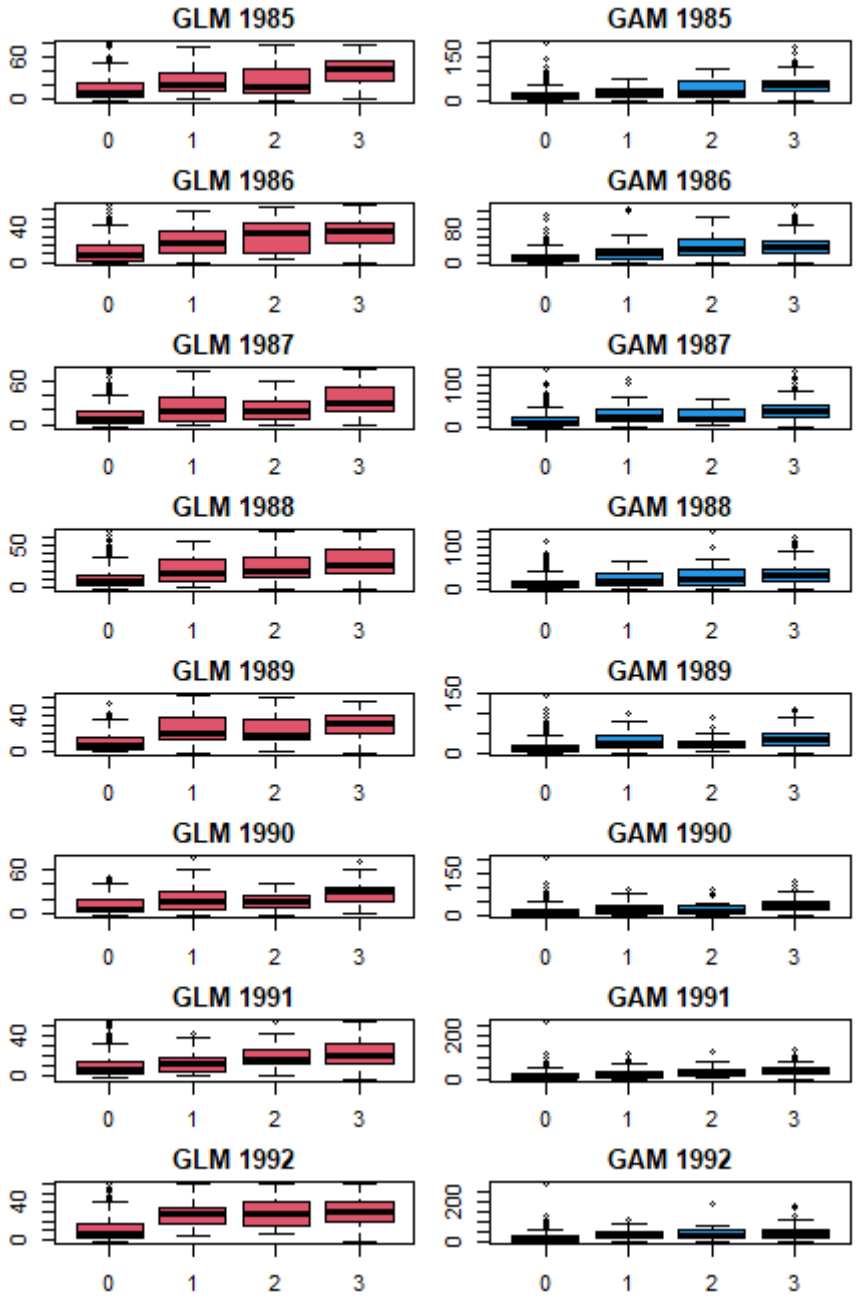
GLM 1985
GAM 1985
GLM 1986
GAM 1986
GLM 1987
GAM 1987
GLM 1988
GAM 1988
GLM 1989
GAM 1989
GLM 1990
GAM 1990
GLM 1991
GAM 1991
GLM 1992
GAM 1992

Fig. 54. (Cont'd)

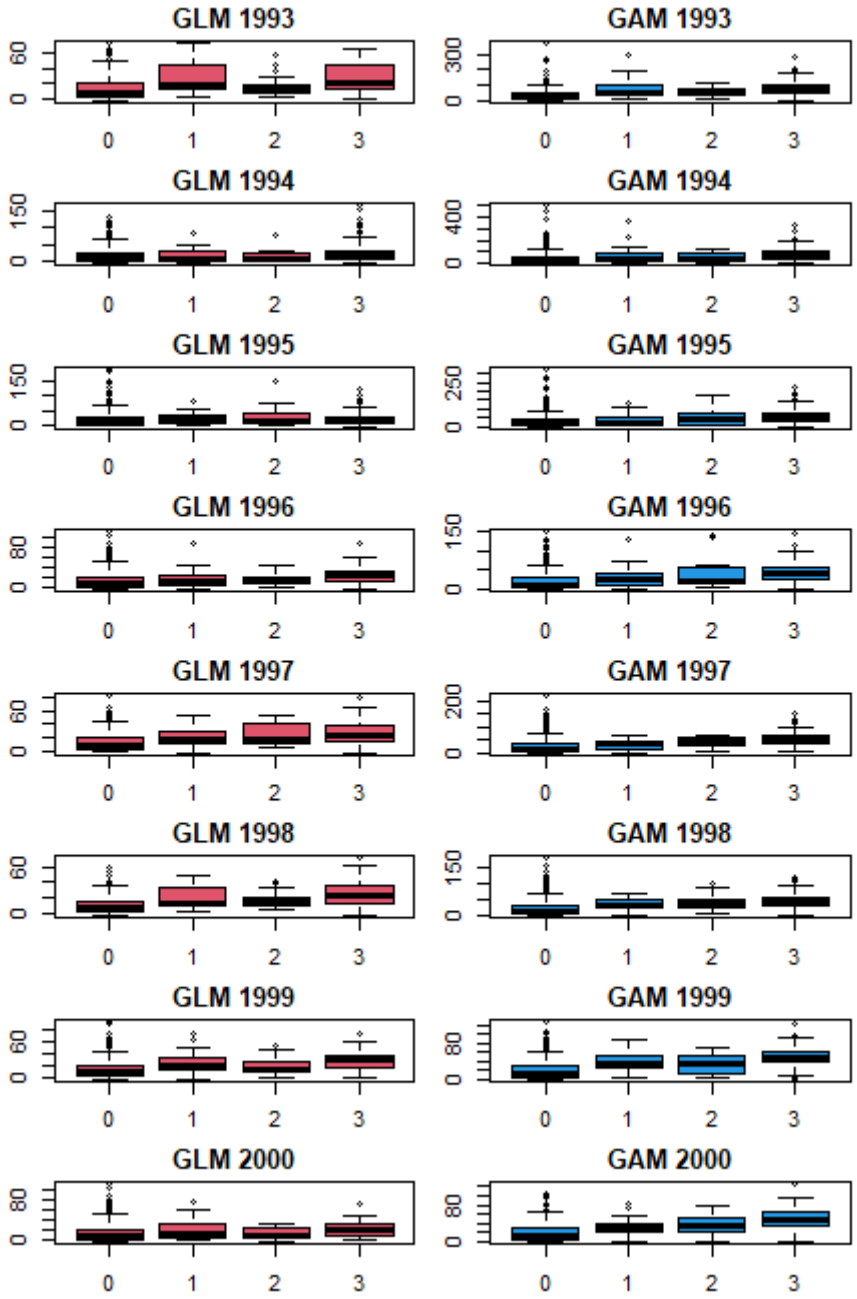
GLM 1993
GAM 1993
GLM 1994
GAM 1994
GLM 1995
GAM 1995
GLM 1996
GAM 1996
GLM 1997
GAM 1997
GLM 1998
GAM 1998
GLM 1999
GAM 1999
GLM 2000
GAM 2000

Fig. 54. (Cont'd)

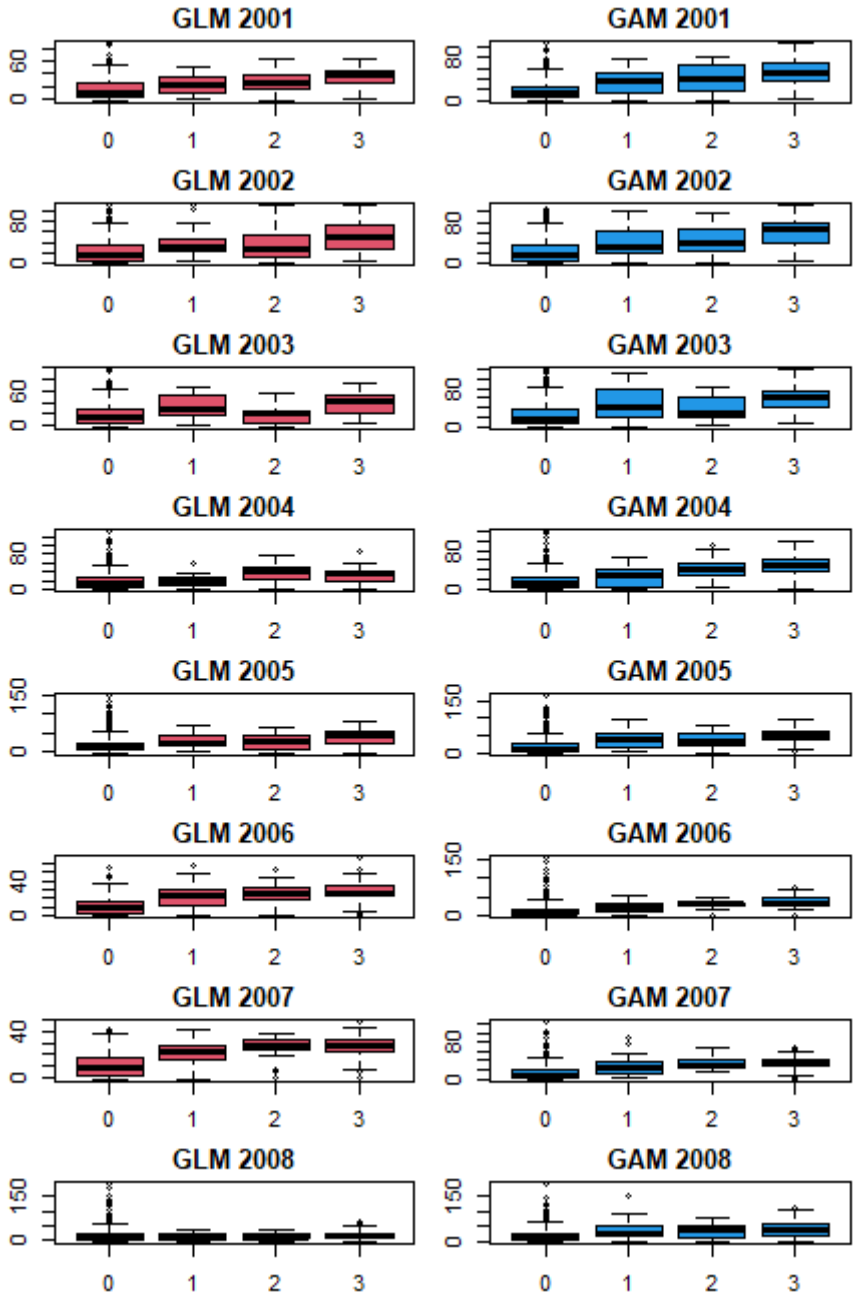
GLM 2001
GAM 2001
GLM 2002
GAM 2002
GLM 2003
GAM 2003
GLM 2004
GAM 2004
GLM 2005
GAM 2005
GLM 2006
GAM 2006
GLM 2007
GAM 2007
GLM 2008
GAM 2008
0
1
2
3

Fig. 54. (Cont'd)

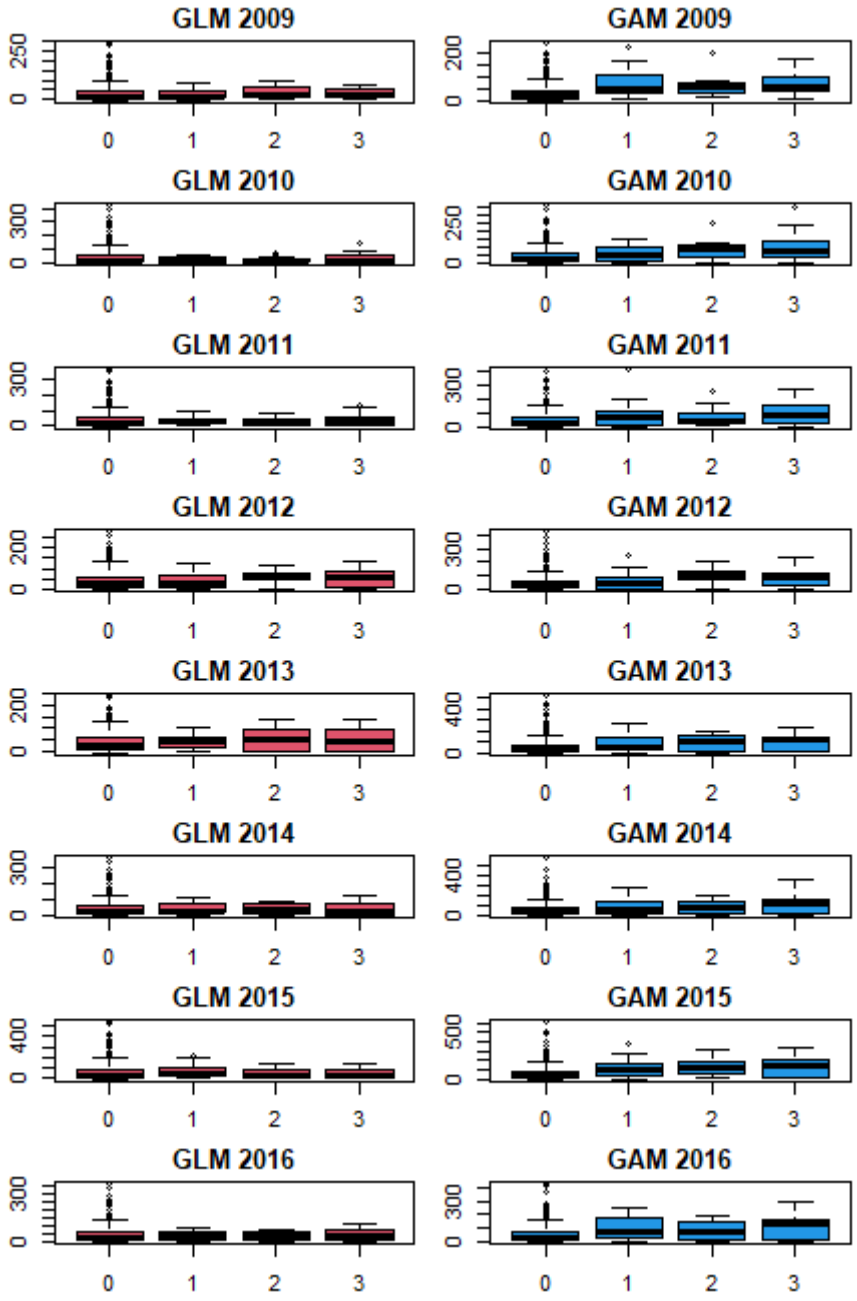
GLM 2009
GAM 2009
GLM 2010
GAM 2010
GLM 2011
GAM 2011
GLM 2012
GAM 2012
GLM 2013
GAM 2013
GLM 2014
GAM 2014
GLM 2015
GAM 2015
GLM 2016
GAM 2016

Fig. 54. (Cont'd)

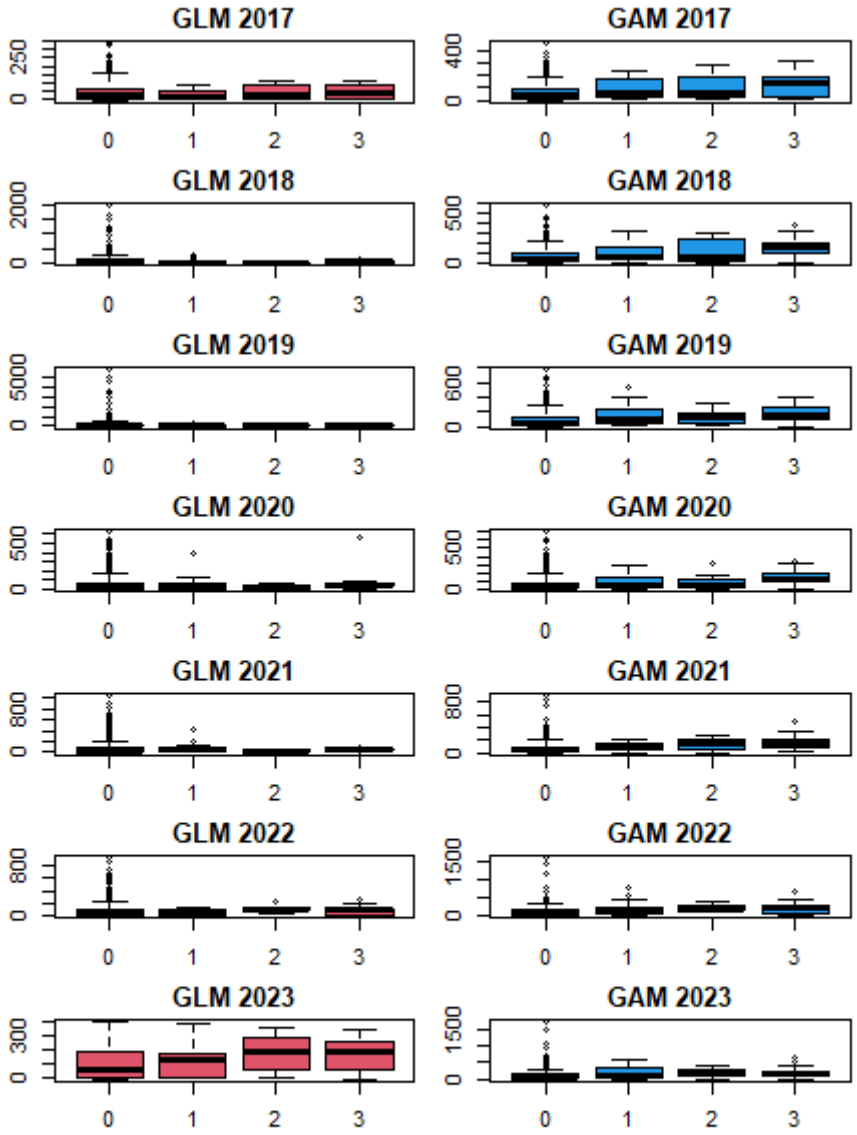
GLM 2017
GAM 2017
GLM 2018
GAM 2018
GLM 2019
GAM 2019
GLM 2020
GAM 2020
GLM 2021
GAM 2021
GLM 2022
GAM 2022
GLM 2023
GAM 2023
0
1
2
3

Fig. 54. (Cont'd)

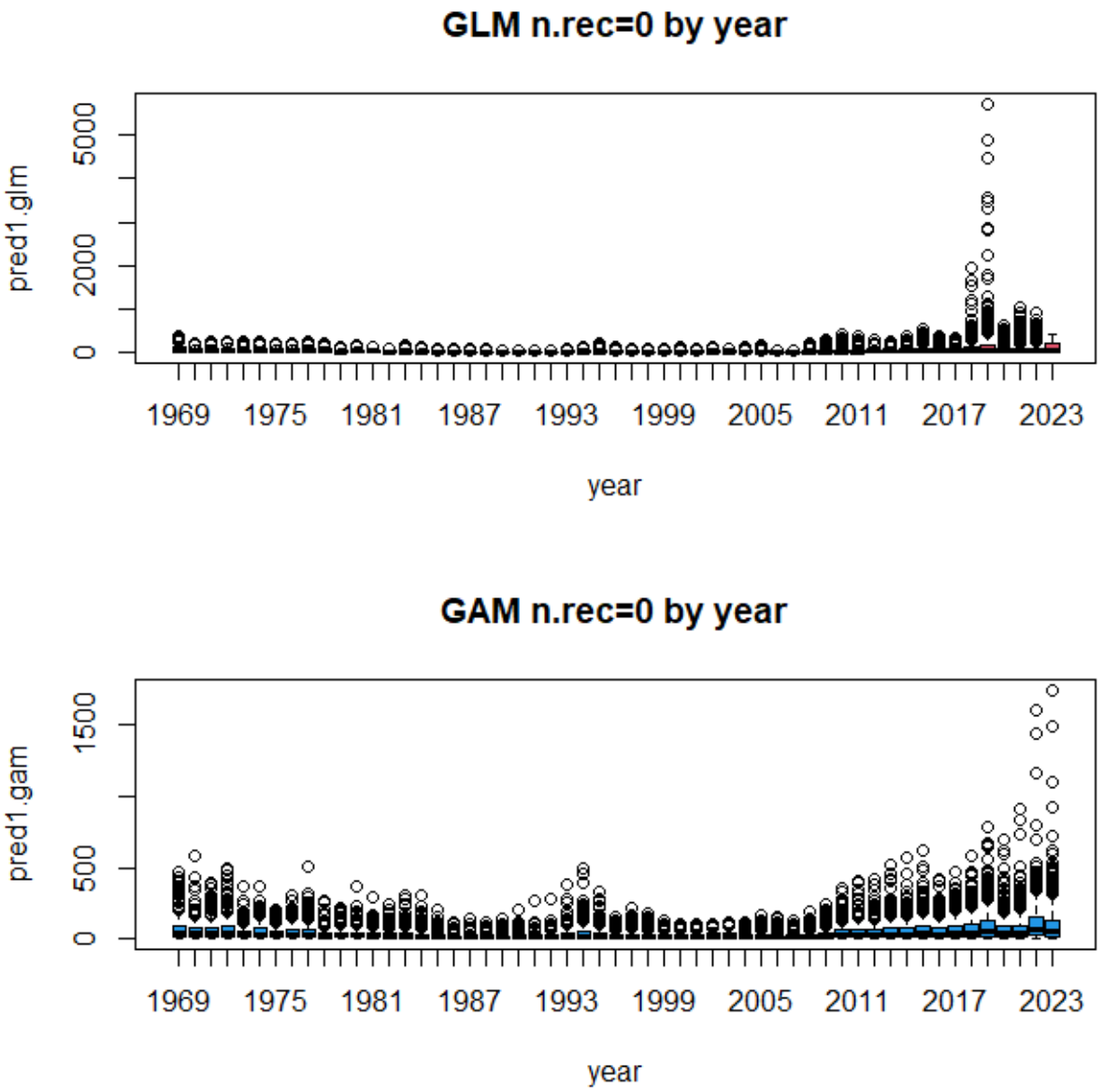

Fig. 55. Boxplot of CPUE predicted values by year in group 0, which no actual data corresponded.

Table 1. The k values selected for each of sub-model.

Submodel	BSM	PCSM
k.month11	5	6
k.lon11	20	20
k.lat11	4	4
k.year24	10	20
k.year25	10	20
k.year26	10	20
k.month22	5	6
k.month23	5	6
k.month26	5	6
k.lon21	10	20
k.lon23	10	20
k.lon25	10	20
k.lat21	4	4
k.lat22	4	4
k.lat24	4	4
k.year31		20
k.year33		20
k.year34		20
k.month31		6
k.month32		6
k.month34		6
k.lon32		20
k.lon33		20
k.lon34		20
k.lat31		4
k.lat32		4
k.lat33		4

Table 2. Statistics of choosing k values in the two sub-models of GAM.

BSM

Term	k'	edf	k-index	p-value
ti(month)	4	3.76	0.9774	0.24
ti(lon.cnt)	19	18.63	0.9672	0.12
ti(lat)	3	2.15	0.9833	0.35
ti(lon.cnt,lat)	27	18.70	0.9603	0.15
ti(month,lat)	12	8.48	0.9435	0.02
ti(lon.cnt,month)	36	31.32	0.9182	0.00
ti(year,lat)	27	22.17	0.9445	0.09
ti(year,lon.cnt)	81	73.71	0.9057	0.00
ti(year,month)	36	34.12	0.9447	0.06
s(log(hook))	9	8.27	0.9959	0.76

PCSM

Term	k'	edf	k-index	p-value
ti(month)	5	4.68	1.0140	0.84
ti(lon.cnt)	19	18.14	0.9997	0.51
ti(lat)	3	2.97	1.0201	0.95
ti(lon.cnt,lat)	42	33.54	1.0092	0.77
ti(month,lat)	14	10.91	1.0130	0.86
ti(lon.cnt,month)	94	72.10	1.0038	0.68
ti(year,lat)	57	47.36	0.9775	0.09
ti(year,lon.cnt)	335	255.46	0.9864	0.14
ti(year,month)	95	79.61	0.9929	0.30
ti(lat,month,year)	155	112.91	0.9637	0.03
ti(lat,lon.cnt,month)	80	60.62	0.9989	0.48
ti(lat,lon.cnt,year)	290	233.83	0.9653	0.01
ti(year,lon.cnt,month)	770	581.39	0.9466	0.00
s(log(hook))	9	7.63	1.0021	0.56

Table 3. Diagnostic statistics of GAM.

Sub-model	BSM	PCSM
n.data	803,439	710,182
dev.expl	73.74%	49.47%
AIC	152,044	1,508,004
residual.df	803,160	708,603
REMLscore	1,547,516	380,028

Table 4. Abundance index as the base case.

Year	Index
1969	2.48230
1970	2.00741
1971	1.77994
1972	1.89907
1973	1.29904
1974	1.55466
1975	1.13866
1976	1.42075
1977	1.36457
1978	0.99399
1979	1.03800
1980	1.08619
1981	0.95992
1982	0.79580
1983	0.87159
1984	0.75089
1985	0.54882
1986	0.42659
1987	0.44153
1988	0.43591
1989	0.42556
1990	0.44590
1991	0.44328
1992	0.55244
1993	0.85266
1994	0.89398
1995	0.68572
1996	0.51090
1997	0.56282
1998	0.52322
1999	0.51164
2000	0.48019
2001	0.47739
2002	0.56149
2003	0.57620
2004	0.42800
2005	0.47647
2006	0.34748
2007	0.35257
2008	0.47444
2009	0.69502
2010	0.93409
2011	0.96569
2012	0.94455
2013	1.13823
2014	1.20047
2015	1.50305
2016	1.20953
2017	1.39743
2018	1.65992
2019	1.95994
2020	1.50932
2021	1.52783
2022	2.39803
2023	2.07894

Table 5. Results of sensitivity analysis for model selection in the binomial sub-model.

name	term	dev.expl	AIC	residual.df	REMLscore	dAIC
modA2	Main and 2 way interactions	73.74%	152,044	803,160	1,547,516	2,682
modA2.no5	-ti(lon, lat)	73.27%	154,720	803,177	3,986,110	5,358
modA2.no6	-ti(month, lat)	73.48%	153,524	803,167	4,415,553	4,162
modA2.no7	-ti(lon, month)	73.42%	153,843	803,190	1,598,090	4,481
modA2.no8	-ti(year, lat)	73.09%	155,750	803,180	2,623,613	6,388
modA2.no9	-ti(year, lon)	72.34%	159,966	803,233	1,469,867	10,604
modA2.no10	-ti(year, month)	72.79%	157,464	803,193	1,296,485	8,102
modA2.no15	-cl	71.07%	167,495	803,159	2,416,441	18,133
modA2.no16	-s(log(hook))	73.38%	154,148	803,168	1,622,046	4,786
modA1	Main effects	67.16%	189,631	803,347	1,256,863	40,269
modA2.p11	+ti(lat, month, year)	74.15%	149,764	803,134	11,097,940	402
modA2.p12	+ti(lat, lon, month)	74.02%	150,535	803,132	521,972,038	1,173
modA2.p13	+ti(lat, lon, year)	73.99%	150,685	803,133	4,189,448	1,323
modA2.p14	+ti(year, lon, month)	74.23%	149,362	803,110	1,087,803	0

Table 6. Results of sensitivity analysis for model selection in the positive catch sub-model.

name	term	dev.expl	AIC	residual.df	REMLscore	dAIC
modB3	Full model	49.47%	1,508,004	708,603	380,028	91
modB3.no5	-ti(lon, lat)	49.45%	1,508,317	708,587	380,187	403
modB3.no6	-ti(month, lat)	49.46%	1,508,105	708,589	380,109	192
modB3.no7	-ti(lon, month)	49.42%	1,508,720	708,562	380,390	807
modB3.no8	-ti(year, lat)	49.47%	1,507,913	708,602	380,018	0
modB3.no9	-ti(year, lon)	49.29%	1,510,493	708,582	380,720	2,579
modB3.no10	-ti(year, month)	49.45%	1,508,204	708,608	380,079	290
modB3.no11	-ti(lat, month, year)	49.45%	1,508,088	708,661	379,987	174
modB3.no12	-ti(lat, lon, month)	49.44%	1,508,339	708,620	380,118	425
modB3.no13	-ti(lat, lon, year)	49.14%	1,512,300	708,777	380,808	4,386
modB3.no14	-ti(year, lon, month)	48.41%	1,521,625	709,144	382,616	13,711
modB3.no15	-cl	49.20%	1,511,797	708,598	380,992	3,884
modB3.no16	-s(log(hook))	49.42%	1,508,646	708,610	380,179	732
modB1	Main effects	41.25%	1,612,039	710,089	403,362	104,126
modB2	Main and 2 way interactions	47.38%	1,534,788	709,548	385,244	26,875

Table 7. Sensitivity analysis of core vessels chosen by various definition.

			Data records			Number of vessels		
Run	xx	yy	Original	core vessel data	%	Original	core vessel data	%
1	9999	1	604,381	604,381	100%	1,680	1,680	100%
2	56	3	604,381	233,542	39%	1,680	286	17%
3	56	5	604,381	164,990	27%	1,680	165	10%
4	56	7	604,381	121,122	20%	1,680	107	6%
5	50	3	604,381	216,523	36%	1,680	262	16%
6	40	3	604,381	182,949	30%	1,680	215	13%
7	30	3	604,381	143,973	24%	1,680	159	9%
8	20	3	604,381	91,357	15%	1,680	93	6%
9	20	5	604,381	57,220	9%	1,680	49	3%

			SBT catch			Run time in minutes			
Run	xx	yy	Original	core vessel data	%	BSM	PCSM	Total	%
1	9999	1	16,821,474	16,821,474	100%	3.47	7.47	10.93	100%
2	56	3	16,821,474	9,780,839	58%	1.46	2.92	4.38	40%
3	56	5	16,821,474	7,416,073	44%	1.01	1.90	2.91	27%
4	56	7	16,821,474	5,834,742	35%	0.82	1.54	2.36	22%
5	50	3	16,821,474	9,368,727	56%	1.34	2.54	3.87	35%
6	40	3	16,821,474	8,381,066	50%	1.15	2.34	3.49	32%
7	30	3	16,821,474	7,082,717	42%	0.96	1.81	2.77	25%
8	20	3	16,821,474	5,190,124	31%	0.62	0.96	1.58	14%
9	20	5	16,821,474	3,542,045	21%	0.37	0.64	1.01	9%

Table 8. Summary statistics of the estimates where CPUE predicted value > 1500, in group 0 in the GLM model.

Year	Area	Month	N	Mean	Max	Sum
2018	8	6	4	1,521	1,521	6,083
2018	8	7	4	1,662	1,662	6,647
2018	8	8	4	1,944	1,944	7,778
2019	8	6	20	2,810	4,481	56,207
2019	8	7	12	3,828	4,896	45,934
2019	8	8	12	4,265	5,728	51,182
2019	8	9	8	1,765	1,765	14,122

Table 9. Summary statistics of the estimates where CPUE predicted value > 800, in group 0 in the GAM_new model.

Year	Area	Month	N	Mean	Max	Sum
2021	4	8	4	830	830	3,319
2021	4	9	4	907	907	3,626
2022	4	8	4	1,443	1,443	5,772
2022	4	9	8	1,389	1,612	11,113
2023	4	7	4	926	926	3,706
2023	4	8	4	1,490	1,490	5,960
2023	4	9	8	1,424	1,749	11,391